Pergamon

Geochimica et Cosmochimica Acta, Vol. 67, No. 24, pp. 4857–4879, 2003

0016-7037/03 $30.00 + .00

doi:10.1016/j.gca.2003.08.012

Northwest Africa 773: Lunar mare breccia with a shallow-formed olivine-cumulate component, inferred very-low-Ti (VLT) heritage, and a KREEP connection

Bradley L. Jolliff,* Randy L. Korotev, Ryan A. Zeigler, and Christine Floss

Department of Earth and Planetary Sciences and The McDonnell Center for the Space Sciences, Washington University, Campus Box 1169, One Brookings Drive, St. Louis, MO 63130, USA

(*Received April* 1, 2003; *accepted in revised form August* 29, 2003)

Abstract—Lunar meteorite Northwest Africa 773 (herein referred to as NWA773) is a breccia composed predominantly of mafic volcanic components, including a prominent igneous clast lithology. The clast lithology is an olivine-gabbro cumulate, which, on the basis of mineral and bulk compositions, is a hypabyssal igneous rock related compositionally to volcanic components in the meteorite. The olivine-gabbro lithology exhibits cumulus textures and, in our largest section of it, includes some 48% olivine (Fo_{64} to Fo_{70}, average Fo_{67}), 27% pigeonite ($En_{60}Fs_{24}Wo_{16}$ to $En_{67}Fs_{27}Wo_{6}$), 11% augite ($En_{50}Fs_{17}Wo_{33}$ to $En_{47}Fs_{13}Wo_{40}$), 2% orthopyroxene ($En_{70}Fs_{26}Wo_{4}$), 11% plagioclase (An_{80} to An_{94}), and trace barian K-feldspar, ilmenite, Cr-spinel, RE-merrillite, troilite, and Fe-Ni metal. The Mg/Fe ratios of the mafic silicates indicate equilibration of Fe and Mg; however, the silicates retain compositional variations in minor and trace elements that are consistent with intercumulus crystallization. Accessory mineralogy reflects crystallization of late-stage residual melt. Both lithologies (breccia and olivine cumulate) of the meteorite have very-low-Ti (VLT) major-element compositions, but with an unusual trace-element signature compared to most lunar VLT volcanic compositions, i.e., relative enrichment in light REE and large-ion-lithophile elements, and greater depletion in Eu than almost all other known lunar volcanic rocks. The calculated composition of the melt that was in equilibrium with pyroxene and plagioclase of the cumulate lithology exhibits a KREEP-like REE pattern, but at lower concentrations. Melt of a composition calculated to have been in equilibrium with the cumulate assemblage, plus excess olivine, yields a major-element composition that is similar to known green volcanic glasses. One volcanic glass type from Apollo 14 in particular, green glass B, type 1, has a very low Ti concentration and REE characteristics, including extremely low Eu concentration, that make it a candidate parent melt for the olivine-gabbro cumulate. We infer an origin for the parent melt of NWA773 volcanic components by assimilation of a trace-element-rich partial or residual melt by a magnesian, VLT magma deep in the lunar crust or in the mantle prior to transportation to the near-surface, accumulation of olivine and pyroxene in a shallow chamber, eruption onto a volcanic surface, and incorporation of components into local, predominantly volcanic regolith, prior to impact mixing of the volcanic terrain and related hypabyssal setting, and ejection from the surface of the Moon. Volcanic components such as these probably occur in the Oceanus Procellarum region near the site of origin of the green volcanic glasses found in the Apollo 14 regolith.

1. INTRODUCTION

Northwest Africa 773, found in September 2000 (Grossman and Zipfel, 2001), is one of the most unusual lunar meteorites to be discovered in recent years. What makes it unusual is that it is a very-low-Ti (VLT) mafic volcanic breccia with relatively high incompatible-trace-element concentrations and LREE/HREE enrichment (Korotev et al., 2002), and that it contains a prominent clast lithology, which is an olivine-rich cumulate (Fagan et al., 2001, Korotev et al., 2002, Bridges et al., 2002). A lunar origin was determined by Fagan and coworkers (Fagan et al., 2001, 2003) from noble-gas contents, oxygen isotopes, and mineral compositions, and a high solar-wind component indicates that at least a part of this meteorite derives from the regolith (see also Eugster and Lorenzetti, 2001). Fagan et al. (2003) describe two lithologies: (1) a "polymict, fragmental regolith breccia" and (2) a cumulate olivine gabbro. In this paper, we refer to these as the breccia (Bx) lithology and the olivine-cumulate (OC) lithology.

The impact breccia components are predominantly volcanic (basaltic), and, in this context, the cumulus lithology is especially significant. Is the cumulate related to the volcanic components or does it represent a deep-seated rock entrained by a basaltic magma as the magma rose to the surface, i.e., might it be a mantle- or deep-crustal xenolith component? Elevated incompatible-element concentrations with more or less KREEP-like interelement ratios, coupled with very low Ti contents, distinguish this meteorite from other mare basalts. Although a few fragments of basalt from Apollo 14 have low Ti and KREEP-like incompatible-element signatures, none of these has the high Fe content of NWA773. Some of the volcanic glasses found at the Apollo 14 site, however, do have these trace- and major-element characteristics.

We previously presented the results of bulk compositional analysis of NWA773 by INAA and preliminary petrographic information (Korotev et al., 2002). Here, we present detailed results of mineral analyses done by electron- and ion-microprobe methods in addition to the compositional data determined by INAA, and we describe the textures and mineral proportions observed in the OC lithology. We focus on OC because of its potential significance as a product of a petrogenetic setting that

* Author to whom correspondence should be addressed (blj@levee.wustl.edu).

has as yet yielded few similar or related samples. Also, the cumulate lithology combines magnesian major-element compositions with a relatively trace-element-rich signature, similar to the lunar magnesian-suite rocks, the petrogenesis of which remains speculative. The reader is referred to Fagan et al. (2003) for a more detailed description of the clast components of the NWA773 breccia lithology.

In terms of the cumulate character of the OC lithology, we consider two hypotheses for its origin: (1) that it is petrogenetically related to the other basaltic components in the meteorite, i.e., that it is a shallow-formed cumulate, perhaps associated with a mare region, and (2) that it represents a deeply formed rock of the middle to lower crust or mantle. Our preliminary compositional and petrographic data, presented in abstract form (Korotev et al., 2002), indicated that the cumulus lithology is indeed related to the basaltic components of the breccia and that it formed in a shallow, not deep setting. In this paper, we compare the compositions of both lithologies (cumulus and breccia) of NWA773 to compositions of other mafic lunar meteorites and to other basaltic compositions known from the Apollo samples. In particular, a volcanic glass from Apollo 14 has a composition that could be related to NWA773, and we explore a petrogenetic scenario for their relationship.

2. SAMPLE SUBDIVISION

This study combines results obtained by three different analytical methods: instrumental neutron activation analysis (INAA), electron-microprobe (EMP) analysis, and ion-microprobe (IMP) analysis. We obtained 712 mg of material in 2 primary samples from the Natural History Museum of London. Subsample designations in the following descriptions correspond to those listed in the tables. One of the primary samples (sample "a") consisted primarily of pieces of the breccia lithology (10 fragments, 284 mg) and the other (sample "b") consisted largely of olivine-cumulate clast material (6 fragments, 408 mg). A third sample, designated "c," weighed 20 mg and consisted primarily of crumbs of the olivine-cumulate material. We further subdivided these samples so as to obtain splits that would represent, with as little mixing and apparent terrestrial contamination as possible, the two main lithologies, as well as some mixed splits and others containing apparent terrestrial contamination, e.g., carbonate deposits (Fig. 1, exterior). Some of these splits were designated for INAA and others for polished probe mounts and fused beads for major-element analysis (see below). Small particulate materials remaining after subdivision were used for three of the fused beads (labeled as "crumbs" in Table 1).

Sample "a" was split in the following manner. Photodocumentation of the rock fragment subdivision is available from the first author upon request: The largest fragment, a1 (84.2 mg) was potted in epoxy using vacuum impregnation and sawn and polished as a probe mount. Fragment a2 (55.2 mg) had an exterior surface or exposed fracture surface with a carbonate deposit, and it had a sawn surface. This fragment was broken into four pieces plus crumbs, with most of the carbonate material on one of the fragments, which was set aside. Sample a2a consisted of breccia matrix plus a 1×1.5 mm clast of OC and a sawn surface. Sample a2b combined two fragments of breccia matrix. Crumbs from this split were combined with other

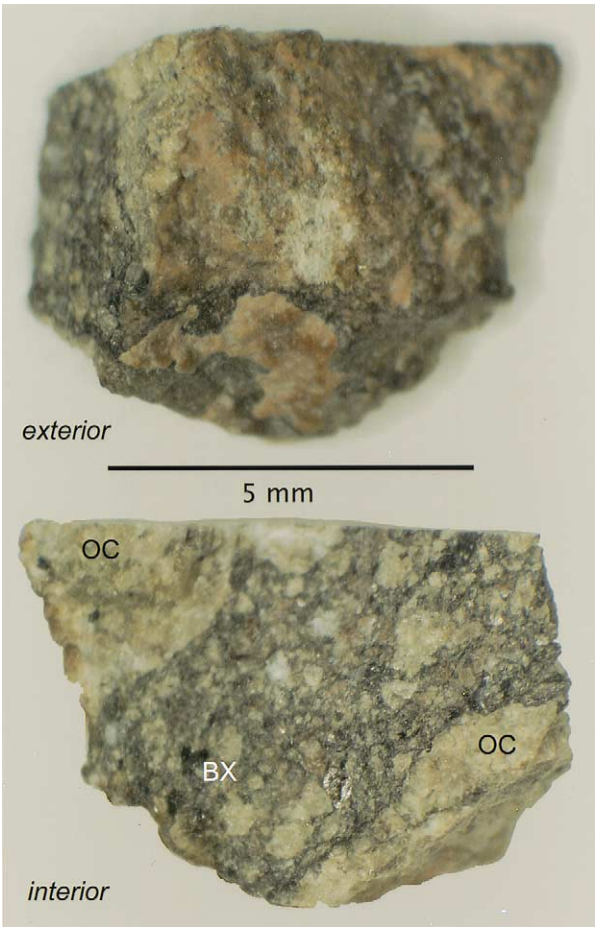

Fig. 1. Macroscopic photo of large fragment of NWA773 (fragment b1). Section shown in Fig. 2 was made from this piece. Pinkish material on rock chip exterior is Ca-carbonate. Two main interior lithologies are olivine-gabbro cumulate (OC) and basaltic breccia matrix (BX).

sample "a" crumbs and made into two fused beads. Sample a3 (23.5 mg) contained breccia matrix and a reddish, smooth surface resembling fusion crust. This sample was encapsulated whole for INAA. Sample a4 (34.8 mg) appeared to have some alteration on one sawn surface and one side appeared to be covered with reddish, glassy fusion crust. We broke this fragment into two pieces plus crumbs: the larger piece, a4a (20.5 mg), which contained what appeared to be fusion crust, and a black, conchoidally fractured interior surface, was selected for INAA, and a4b (10.9 mg) was made into two fused beads. Sample a5 (16.4 mg) had reddish alteration on one end and some very fine-scale drusy carbonate coating plus a sawn surface; we crushed the entire fragment and made two fused beads from it. Sample a6 (14.0 mg) appeared to have some fusion crust and some relatively coarse (750 μm) plagioclase clasts; this sample was reserved. Sample a7 (13.9 mg) appeared to have reddish oxide alteration on one end and had a sawn surface; it was crushed for FB analysis. Sample a8 (14.3 mg) is breccia matrix (with no apparent surfaces), but also had reddish coloration on one end. This sample was analyzed by INAA. Sample a9 (10.5 mg) consists of light-colored, plagioclase-rich, breccia matrix with some carbonate deposits; this sample was

Table 1. NWA773 major element compositions, determined by fused bead electron microprobe analysis.

	Subsample Analyses						Lithology Averages[d]			
split[a]	a-crumbs[b]	a4	a5	a7	b-crumbs	b6	c-crumbs	Breccia	Olivine	Olivine
#spots	17	19	17	16	25	16	8	Matrix	Cumulate	Cumulate
#beads	2	2	2	2	3	2	1	8	5	MR[f]
SiO_2	45.7	46.1	45.5	48.0	44.7	44.9	43.5	46.2	44.8	44.8
TiO_2	0.87	0.74	0.70	0.70	0.20	0.32	0.22	0.78	0.24	0.31
Al_2O_3	10.0	9.7	13.6	10.7	3.5	2.7	3.1	10.6	3.1	3.8
Cr_2O_3	0.38	0.41	0.38	0.46	0.42	0.33	1.09	0.40	0.39	0.40
FeO	18.1	18.2	15.8	16.4	18.0	18.2	19.9	17.3	18.1	18.0
MnO	0.28	0.28	0.19	0.29	0.28	0.25	0.28	0.26	0.27	0.25
MgO	13.6	13.6	11.6	13.9	26.9	27.4	27.7	13.2	27.1	25.4
CaO	10.6	10.8	12.0	9.52	6.03	5.99	4.84	10.8	6.01	6.27
Na_2O	0.20	0.22	0.27	0.23	0.03	0.03	0.05	0.23	0.03[e]	0.11
K_2O	0.09	0.11	0.10	0.11	0.02	0.03	0.05	0.10	0.02	0.09
P_2O_5	0.10	0.10	0.09	0.08	0.04	0.06	0.05	0.09	0.05	0.05
Sum Oxides[c]	99.9	100.2	100.3	100.4	100.1	100.2	100.9	100.1	100.1	99.5
Mg/(Mg + Fe)	0.57	0.57	0.57	0.60	0.73	0.73	0.71	0.58	0.73	0.72
Ca/Al molar	1.9	2.0	1.6	1.6	3.1	4.0	2.8	1.8	3.5	3.0

[a] Splits labelled "a" are mostly breccia matrix (Bx) lithology. Splits b and c consist mostly of olivine cumulate (OC) lithology.
[b] Crumbs are fragments left after dividing splits into subsamples.
[c] Molybdenum normalized out. Average Mo (mostly as metal) in bead analyses: 0.5 wt.%.
[d] Average compositions are weighted according to standard deviations of bead analyses.
[e] Na_2O by INAA = 0.13. Na_2O by FB-EMPA suffers volatilization (see text).
[f] MR: modal recombination (see Table 2).

also analyzed by INAA. Sample a10 (7.8 mg) appears to have abundant carbonate on one side; it was held in reserve. Combined crumbs from splitting the "a" samples were made into two fused beads.

Sample "b" was split as follows: The largest fragment, b1 (199 mg), was potted in epoxy using vacuum impregnation and sawn and polished as a probe mount. Fragments a1 and b1 were mounted together and were large enough that two potted mounts remain after sawing. Fragment b1 was composed mostly of dark, crystalline clast-rich matrix, but with two large clasts of the light-green, coarsely crystalline OC lithology (Fig. 1). Sample b2 (61.9 mg) consisted almost entirely of the OC lithology and was subdivided into two fragments plus crumbs for analysis. The two fragments, b2a and b2b, were analyzed separately by INAA. Remaining crumbs were added to b crumbs for FB analysis. Sample b3 (54.2 mg) consisted of about 80% OC clast and 20% of glassy material that appeared to be fusion crust with some reddish alteration. This sample was split into a fragment for INAA and the remainder was combined with the b crumbs. Sample b4 (36.9) consists of OC material, breccia matrix, glassy surface (fusion crust?), and a sawn edge; it was held in reserve. Sample b5 (33 mg) appeared to be unaltered and consisted of about 60% OC and 40% breccia matrix, with one sawn surface and apparently a large chromite grain. This fragment was analyzed by INAA. It was anticipated that samples b3 and b5 (especially the latter) would provide intermediate compositions that would lie along mixing lines between the two main lithologies. Sample b6 (20.2 mg) consisted of mostly green OC clast material with only a slight amount of reddish coloration; it was subdivided into material for two fused beads. Crumbs left from processing "b" samples were made into three fused beads, and the "c" crumbs (separate split) were made into 2 fused beads.

3. ANALYTICAL METHODS

Subsampled rock fragments for INAA were sealed using an oxygen-methane torch into high-purity silica tubes for neutron irradiation. Samples were irradiated in the research reactor at the University of Missouri, Columbia, at a thermal-neutron flux of $5.15 \times 10^{13} cm^{-2} s^{-1}$ for 36 h. Radioassays were done 6 d following removal from the reactor, and again at 7–9, 10–12, and 23–29 d following the irradiation. We used a combination of well known rock and synthetic glass standards, following procedures given in more detail by Korotev (1991). In all of our REE plots, concentrations are normalized to those in chondritic meteorites as given by Anders and Grevesse (1989) times a factor of 1.36, which gives a value of Sm = 0.2000 μg/g for self-consistency with previously published INAA results (e.g., Jolliff et al., 1991, 1998; Korotev, 1991, 1996).

Electron-microprobe analyses were done using the JEOL733 Superprobe equipped with Advanced Microbeam Inc™ automation at Washington University. All mineral analyses were done using wavelength-dispersive spectrometers operating at 15 kV accelerating voltage and using a 20 nA beam current for feldspars and 30 nA for other minerals. Beam diameters of 10–20 μm were used to obtain integrated analyses of finely exsolved pyroxene grains; 5–10 μm for feldspar grains, and 1–10 μm for olivine, phosphates, oxides, and metal. A combination of silicate and oxide mineral standards were used for calibration of silicates, mostly oxide standards for spinel and ilmenite, and metal and phosphide standards for Fe-Ni metal. Data reduction was done using *Probewin* from Advanced Microbeam Inc., which incorporates X-ray matrix corrections according to a modified (Armstrong, 1988) CITZAF routine.

Fused beads for major-element analysis by electron microprobe (FB-EMPA) were prepared using a molybdenum-strip resistance heater, following crushing in an agate mortar, using methods described by Jolliff et al. (1991). Fusions were done in an Ar atmosphere. Analyses were made on the polished glasses using standard wavelength-dispersive EMP procedures with the JEOL733 electron microprobe. We used basaltic glass standards for Si, Al, Fe, Mg, and Ca, and we used rutile for Ti, Cr oxide for Cr, rhodonite for Mn, orthoclase for K, albite for Na, and apatite for P. According to many analyses of fused beads by this method, we find that volatilization is usually a problem only for Na, and that concentrations of Na by FB-EMPA typically are about 5–10% less than by INAA. In our preparation of NWA773, however, we found that the OC lithology required a somewhat stronger

heat pulse to fuse than typical, so the Na_2O values reported for the fused bead analyses may represent significantly more volatilization than typical (Fagan et al., 2003, also reported difficulty fusing the OC lithology). Fused-bead compositions typically contain less than 1 wt.% of molybdenum as MoO. Compositions of fused beads prepared from subsamples of OC were very similar for beads prepared from individual subsamples as well as those prepared from other subsamples, indicating that our average OC composition probably approaches a representative composition for this lithology (Table 1: b crumbs, b6, and c crumbs).

The concentrations of REE and other trace elements were measured in NWA773 OC silicates and RE-merrillite using a modified Cameca 3-f ion microprobe according to methods given in Zinner and Crozaz (1986). Details of the experimental and data-reduction procedures are given by Floss (2000). To make interference corrections and to assess possible terrestrial contamination and overlaps between phases, we measured at masses corresponding to Na, Mg, Si, P, S, K, Ca, Sc, Ti, V, Cr, Mn, Fe, Co, Ni (olivine only), Rb, Sr, Y, Zr, Ba, La, Ce, Pr, Nd, Sm, Eu, Gd, Tb, Dy, Ho, Er, Tm, Yb, and Lu. All measurements were normalized using Si as the reference element for silicates and Ca for RE-merrillite; Si and Ca concentrations were determined by EMP analyses of the same grains and in approximately the same spots as analyzed with the ion microprobe.

In this paper, we use *RE-merrillite* instead of *whitlockite*, following the suggestion of Rubin (1997) because the structure of this lunar phosphate is better understood in terms of meteoritic merrillite than terrestrial whitlockite (Jolliff et al., 1993).

4. MINERAL ASSEMBLAGE, MAJOR-ELEMENT COMPOSITION, AND TEXTURES

4.1. Mineral Assemblage

Judging from the material we have studied, NWA773 contains on average about 2/3 basaltic breccia matrix and 1/3 coarse-grained olivine-gabbro cumulate as large lithic clasts (e.g., Fig. 1). The samples we received from the Natural History Museum of London, however, were intended to represent the two main lithologies and are not necessarily expected to represent the proportions of the two main lithologies for the entire meteorite. Killgore (personal communication, 2003) indicates that the bulk meteorite, consisting of three separate stones, contains more of the OC lithology than of Bx. The high proportion of large OC lithic clasts is unusual and makes this meteorite, in a gross sense, a dilithologic breccia. In addition to large lithic clasts of OC, the breccia matrix contains small lithic clasts of OC and of its constituent minerals, and the breccia matrix extends into fractures in large clasts of OC. On a very fine scale, the breccia matrix appears to be glassy, but loaded with abundant, very-fine-grained mineral clasts.

On the basis of our samples, the OC lithology is about half olivine, 35–40% pigeonite+augite, and 10–12% plagioclase (Fig. 2, Table 2). Because of coarse grain size and small samples, modes reported herein as well as by Fagan et al. (2001, 2003), Grossman and Zipfel (2001), and Bridges et al. (2002) vary significantly (Table 2). The low plagioclase content of OC puts the assemblage right at the boundary for nomenclature between olivine gabbro and lherzolite (see Stöffler et al., 1980), but the small size of most fragments makes this distinction academic. On the basis of its mode, the assemblage has excess (cumulus) olivine and probably excess pigeonite, and too little plagioclase for the crystalline equivalent of a reasonable melt composition. Texturally, the cumulus nature of olivine is evident in large, juxtaposed, subhedral to euhedral grains with pyroxene and plagioclase filling interstices (Fig. 3).

In our samples, the breccia contains clasts of the cumulate lithology ranging in size from several millimeters to small, individual mineral clasts. The breccia also contains mineral and lithic clasts of other basaltic lithologies, including strongly zoned pyroxene and olivine that range to high values of Fe/(Mg+Fe); a variety of plagioclase grains, some uniformly anorthitic and others zoned in Na/Ca; fayalite-hedenbergite-silica symplectites; small lithic clasts of fine-grained basalt; and clasts of a late-stage assemblage of silica-K-feldspar-plagioclase intergrowths plus troilite, baddeleyite, and RE-merrillite (Fig. 4). This assemblage of lithic clast material is very similar to that described in EET96008 lunar basaltic breccia (Snyder et al., 1999). Except for the kinds of lithic clasts mentioned above

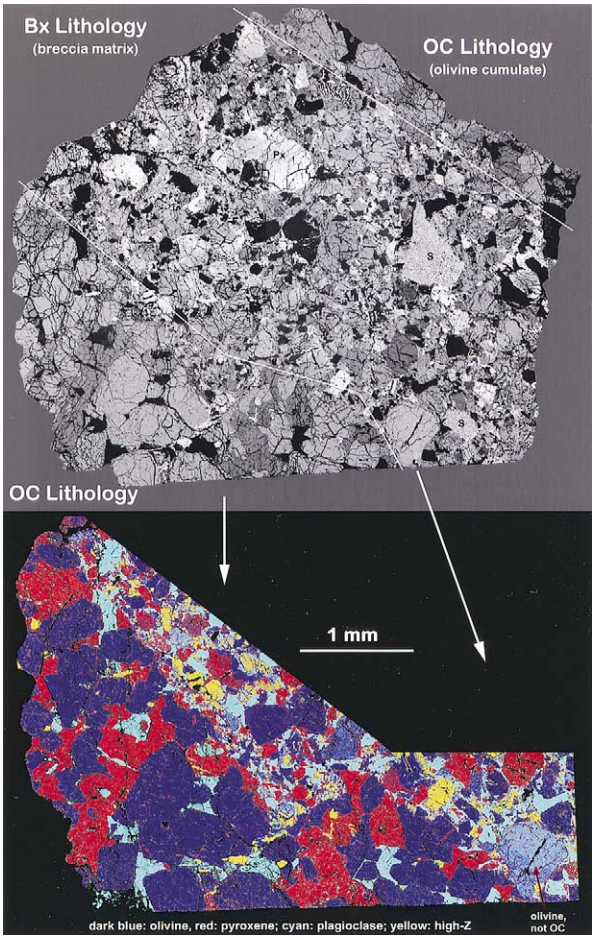

Fig. 2. Backscattered-electron composite image (BSE) of NWA773 b1, large fragment shown in Fig. 1. Olivine-gabbro cumulate (OC) occurs in two large clasts, upper right and lower left. Smaller fragments and mineral grains of OC are scattered within the breccia matrix (Bx). Plagioclase grains are dark and mafic mineral grains vary in brightness mainly according to their Fe content. Large, bright grain in Bx is a zoned pyroxene (px). Several grains of fayalite-hedenbergite-silica symplectite occur on right side of Bx (s). Lower image is false-colored, generated from the BSE, to highlight the major silicate phases of OC, lower-left clast. "High-Z" phases include ilmenite, RE-merrillite, spinel, and other accessory minerals of high mean atomic number. The contact between OC and Bx mineral grains is fairly sharp; however, the breccia matrix is very compact and is composed largely of the same mineral phases as OC. Differences in brightness in BSE, enhanced by false color, show mineral compositional differences that distinguish grains within Bx from those of OC (e.g., olivine grain, lower right).

Table 2. Modal mineralogy of NWA773 olivine-cumulate lithology.

	Mra	mineral composition (this work)			FB Norm[b]	Image Anal[d]	Gros & Zipf[e]	Fagan et al.[f]	Bridges et al.[g]
	vol%	average	Mg′[h]	range	vol%	vol%	vol%	vol%	vol%
Olivine	48	$Fo_{67.5}$	67.5	Mg′ 63–69	48.2	55.0	54.7	55.5	66
Pigeonite	27	$En_{53}Wo_{12}$	71.6	Mg′ 71–72	27.0[c]	|	24.2	18.9	25.9
Augite	11	$En_{49}Wo_{37}$	77	Mg′ 74–79	12.9[c]	31.5	5	8.7	
Orthopyroxene	2	$En_{70}Wo_4$	72			|			
Plagioclase	11	$An_{88}Ab_{10}Or_2$		An 80–94	10.8	12.5	15.6	14.2	8.2
K-Feldspar	tr	$Or_{92}Ab_4An_2Cn_2$			0.17			1.6	tr
Ilmenite	tr				0.33	|	|	0.3	tr
RE-Merrillite	tr				0.12	|	|	<0.2	tr
Troilite	tr					1.0	0.5	tr	tr
Cr-spinel	tr				0.38	|	|	0.9	tr
Fe-Ni metal	tr					|	|	tr	tr

[a]MR: optimized from modal recombination/petrographic image analysis.
[b] FB Norm: normative mineralogy based on Fused Bead analyses, OC lithology.
[c] Pyroxene values for FB Norm are recast in terms of pigeonite and augite of measured wollastonite content instead of "diop" and "hyp" as in standard CIPW calculations.
[d] Average mode from BSE image analysis of 3 clasts of OC. 31.5 = total pyroxene; 12.5 = total feldspar. 1.0 = total high-Z.
[e] Gros & Zipf: Grossman and Zipfel (2001); 15.6 = total feldspar. 0.5 = total opaques.
[f] Fagan et al. (2003) revised slightly from Fagan et al. (2001).
[g] Bridges et al., (2001), pyroxene varieties not distinguished.
[h] Mg′ = Mg/(Mg + Fe) atomic × 100.
Calcite is present as terrestrial contamination at about 1% level, but is not included here.

and shown in Figures 2, 3, and 4, we observed no other prominent lithic clast types in our sections. We did not observe volcanic glass spherules in our sections, although Fagan et al. (2003) reported one aluminous spherule.

At high magnification, the breccia has a glassy matrix that is charged with very-fine-grained clasts and in places the matrix appears to have flowed, reminiscent of pseudotachylite. In at least one instance, we observe very small glassy areas that differ from the typical glassy groundmass in appearance. These areas contain fewer clasts and more vesicles, and resemble agglutinates (Fig. 4f). The occurrence of conchoidal fracture on interior broken surfaces of the breccia matrix reflects its essentially glassy nature.

4.2. Major-Element Composition

Both lithologies of NWA773 have high FeO concentrations. In subsamples analyzed by FB-EMPA, FeO concentrations lie in the range 16.4–18.2 wt.% in the breccia and 18.0–19.9 wt.% in OC (Table 1). In the 10 subsamples analyzed by INAA, FeO concentrations lie in the range 12.3–19.8 wt.% in the breccia and 19.4–20.4 wt.% in OC (Table 3). Subsample a9, which has the lowest FeO concentration among those analyzed by INAA, contains a large plagioclase clast and a fair amount of Ca carbonate. The average FeO concentrations of the splits analyzed by FB-EMPA (17.3±1.2 for Bx and 18.1±1.0 for OC) are less than those analyzed by INAA (18.1±2.8 for Bx and 20.0±0.5 for OC). Fagan et al. (2003) obtained average values of FeO of 19.9 wt.% for the breccia and 19.6 wt.% FeO for the olivine gabbro, and Bridges et al. (2002) reported 19.8 wt.% FeO for the olivine cumulate. Comparison of these values suggests that our FB-EMPA FeO values might be systematically low; for one subsample analyzed by both methods (a4), we obtained FeO values of 18.2 by FB-EMPA and 18.6 by INAA, suggesting that real variability among subsamples also

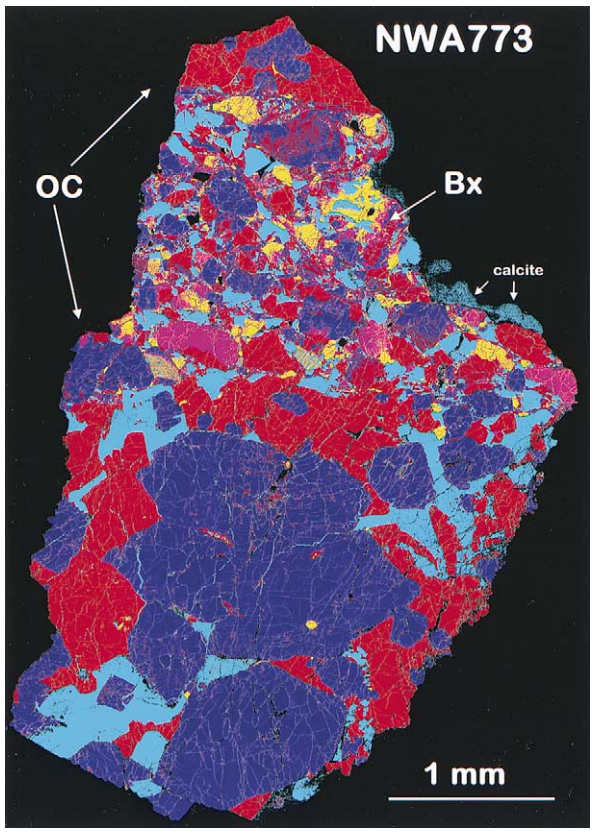

Fig. 3. False-colored backscattered-electron image of a second section made from fragment b1 showing coarse-grained cumulus texture, with pyroxene and plagioclase filling interstices between subhedral to euhedral olivine primocrysts. Within the olivine cumulate (OC), dark blue = olivine, red = pyroxene, cyan = plagioclase, and yellow = high Z phases (spinel, ilmenite, troilite, etc.). At upper right, on the edge of Bx, delicate calcite deposits, which survived the sectioning process, are present.

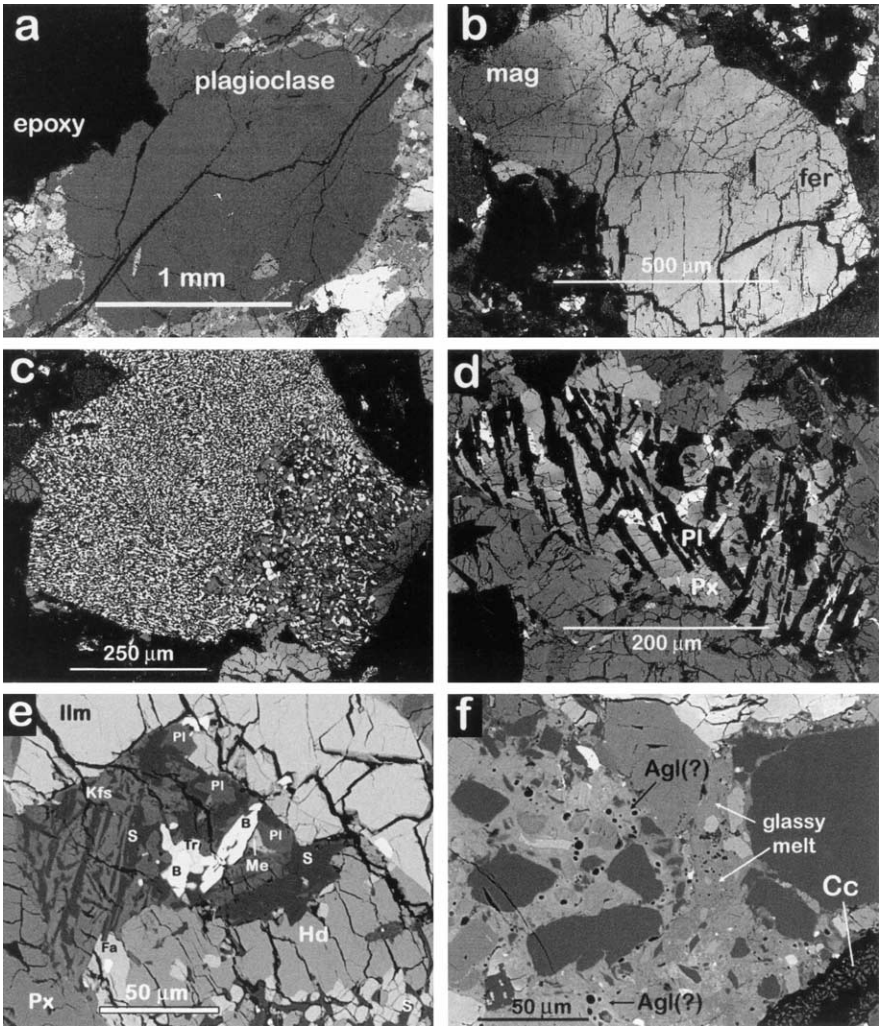

Fig. 4. Breccia components and textures observed in NWA773. (a) coarse plagioclase clast in split a1 (1.2 mm wide by 1.8 mm long); (b) coarse pyroxene clast in split b1 (mag = magnesian, fer = ferroan); (c) symplectite (hedenbergite-fayalite-silica); (d) fine-grained basaltic clast (dark = plagioclase, intermediate = pyroxene, bright = Fe-Ti oxide); (e) silica-K-feldspar granophyre (Kfs –K-feldspar, S – silica, Pl – plagioclase, B – baddeleyite, Ilm – ilmenite, Hd – hedenbergite, Tr – troilite, Fa – fayalite, Me – RE-merrillite); (f) glassy groundmass and possible agglutinate (Agl). Fracture filling in lower-right corner is partially filled with calcite deposits.

contributes to these differences. Our fused bead compositions for the olivine cumulate are also lower in alumina than those reported by Bridges et al. (2002) and Fagan et al. (2003).

The high FeO concentration of the NWA773 breccia coupled with $<$11 wt.% Al_2O_3 in the NWA773 breccia leave little room for contamination by nonvolcanic or "nonmare" or "highland" components. Among observed breccia clasts, nonvolcanic components are scarce: we found no lithic clasts of obvious highland origin, and Fagan et al. (2003) reported only an anorthositic agglutinate and an aluminous, possibly impact-generated glass spherule. Although small segregations of silica-K-feldspar granophyre such as that shown in Figure 4e could be associated with a KREEP or granitic component, we attribute this assemblage to late-stage, relatively evolved differentiates of an anhydrous basaltic/gabbroic magma, as did Fagan et al. (2003). If these late-stage differentiates were associated with a KREEP component, KREEP basalt should also be found as a lithic-clast component and it is not. NWA773 is at the mafic end of the trend of Al_2O_3 vs. FeO+MgO, even compared to other lunar mafic meteorites, consistent with the observed abundance of basaltic or gabbroic components and lack of obviously non-volcanic components.

The normative mineral proportions derived from the major-element composition of OC, as determined by fused bead analysis (Table 1), is generally consistent with the observed mineral proportions. Our largest section of the olivine-gabbro lithology (b1) includes some 48% olivine (Fo_{64} to Fo_{70}, average Fo_{67}), 27% pigeonite ($En_{60}Fs_{24}Wo_{16}$ to $En_{67}Fs_{27}Wo_6$, average $En_{63}Fs_{25}Wo_{12}$), 11% augite ($En_{50}Fs_{17}Wo_{33}$ to $En_{47}Fs_{13}Wo_{40}$, average $En_{49}Fs_{14}Wo_{37}$), 2% orthopyroxene ($En_{70}Fs_{26}Wo_4$), 11% plagioclase (An_{80} to An_{94}), and trace barian K-feldspar, ilmenite, RE-merrillite, Cr-spinel, troilite, and Fe-Ni metal (Table 2). Likewise, a modal recombination using measured mineral compositions (Table 4) produces a

Table 3. Composition of subsamples of NWA773 determined by INAA.

Sample	mg	Na_2O	K_2O	CaO	Sc	Cr	FeO	Co	Ni	Zn	As	Br	Rb	Sr
NWA 773 a2a	22.96	0.22	<1.9	10.3	36.90	2710	19.83	65.3	160	46	<3.0	<2.5	<10	130
NWA 773 a2b	17.42	0.24	<0.7	10.1	39.20	3320	19.65	59.4	100	19	<0.9	<1.6	<6	<150
NWA 773 a3	23.45	0.23	<2.3	12.3	38.20	2810	17.44	54.9	90	38	<1.8	<2.1	<13	100
NWA 773 a4	20.51	0.23	<1.0	10.3	34.10	3190	18.62	62.2	100	<40	<1.2	<1.4	<11	<160
NWA 773 a8	14.28	0.23	<0.6	11.8	38.70	3610	17.94	57.1	140	28	<1.4	<3.0	<7	90
NWA 773 a9	9.60	0.29	<1.2	15.0	35.60	2310	12.30	34.3	80	<21	<1.1	<3.0	<7	90
NWA 773 b2a	27.84	0.13	<0.5	5.7	20.60	1408	19.68	90.4	240	16	<0.7	<0.9	<7	<110
NWA 773 b2b	18.20	0.11	<0.7	5.7	17.76	1303	20.40	94.9	229	16	<0.8	<1.4	<6	50
NWA 773 b3	24.25	0.10	<1.1	5.8	20.60	3480	20.20	92.7	230	22	<1.4	<1.7	<6	<80
NWA 773 b5	33.00	0.17	<1.4	8.1	27.20	6240	19.41	77.1	170	14	<0.8	<1.1	<8	70
Mass-weighted means														
Bx (a subsamples)	108.22	0.24	0.12	11.3	37.1	3004	18.14	58	114	28	0.38	0.4	1.5	96
OC (b2 splits)	46.04	0.13	0.10	5.7	19.5	1366	19.96	92	236	16	0.06	0.2	bd	50
mixed OC & Bx	57.25	0.14	0.12	7.1	24.4	5071	19.74	84	195	17	0.14	0.2	bd	57
Bx-15%OC		0.26	0.12	12.3	40.3	3293	17.81	52	93	30	0.43	0.46	1.5	104

Sample	Zr	Sb	Cs	Ba	La	Ce	Nd	Sm	Eu	Tb	Yb	Lu	Hf
NWA 773 a2a	170	<0.16	<0.40	149	11.5	29.6	19.0	5.46	0.54	1.15	4.05	0.553	4.37
NWA 773 a2b	200	<0.12	0.19	159	16.9	44.4	26.0	7.82	0.58	1.57	5.18	0.701	4.96
NWA 773 a3	180	<0.17	0.17	212	12.4	32.8	19.0	5.89	0.58	1.21	4.27	0.589	4.66
NWA 773 a4	210	<0.13	<0.30	335	16.5	42.9	25.0	7.31	0.69	1.39	4.79	0.646	5.03
NWA 773 a8	180	<0.11	<0.24	177	17.5	45.2	25.0	7.71	0.65	1.57	5.33	0.716	4.51
NWA 773 a9	180	<0.11	<0.40	123	9.9	26.1	17.0	4.63	0.57	0.94	3.38	0.462	3.82
NWA 773 b2a	190	<0.05	<0.19	129	10.8	27.3	16.0	4.49	0.31	0.88	2.78	0.384	4.15
NWA 773 b2b	113	<0.18	<0.22	105	9.0	23.3	12.9	3.81	0.28	0.73	2.39	0.336	3.06
NWA 773 b3	140	<0.08	<0.18	127	9.4	24.5	14.0	4.04	0.25	0.78	2.59	0.359	3.20
NWA 773 b5	120	<0.05	<0.18	121	7.9	20.9	11.0	3.80	0.41	0.80	2.96	0.415	3.05
Mass-weighted means													
Bx (a subsamples)	187	0.03	0.13	201	14.2	36.9	21.9	6.51	0.60	1.31	4.53	0.62	4.62
OC (b2 splits)	160	0.02	0.07	120	10.1	25.7	14.8	4.22	0.29	0.82	2.63	0.37	3.72
mixed OC & Bx	128	0.00	0.05	124	8.5	22.4	12.3	3.90	0.34	0.79	2.80	0.39	3.11
Bx-15%OC	192	0.03	0.14	215	14.9	38.9	23.1	6.91	0.65	1.40	4.87	0.66	4.78

Sample	internal	Ta	W	Ir	Au	Th	U	brief description
NWA 773 a2a	36	0.52	<6	<7	<8	1.79	0.44	matrix + 1 × 1.5 mm OC clast plus sawn face
NWA 773 a2b	37	0.54	<1.9	<5	<7	2.35	0.69	matrix + some exterior surface or frax filling of altered material
NWA 773 a3	45	0.56	<4	<5	5	2.02	0.54	matrix, "clean" interior + fusion crust (?)
NWA 773 a4	40	0.58	<1.8	<5	<8	2.55	0.66	glassy matrix + fusion crust
NWA 773 a8	41	0.59	<3	<5	<9	2.81	0.77	interior matrix frag w/ reddish oxide alteration
NWA 773 a9	42	0.33	<2.5	<5	<7	1.53	0.44	matrix, coarse plag grain, plus carbonate (?)
NWA 773 b2a	38	0.53	<1.1	<4	<4	1.72	0.38	nearly pure OC material
NWA 773 b2b	39	0.33	<1.8	<3	<5	1.36	0.35	nearly pure OC material
NWA 773 b3	43	0.41	<2.4	<3	<4	1.41	0.24	~80% OC lithology + 20% fus crust + alteration
NWA 773 b5	44	0.40	<1.9	<4	<4	1.23	0.31	~60% matrix, 40% OC lithology, chromite; sawn surface
Mass-weighted means								
Bx (a subsamples)		0.54	0.4	0.2	2.1	2.19	0.59	breccia lithology
OC (b2 splits)		0.45	0.0	bd	0.1	1.58	0.37	olivine cumulate lithology
mixed OC & Bx		0.40	0.2	bd	0.6	1.31	0.28	mixed lithologies
Bx-15%OC		0.55	0.4	0.20	2.49	2.29	0.63	

Bx-15%OC calculated as: concentration = (Bx-0.15 × OC)/0.85. Composition is intended to represent breccia matrix minus inferred fine-grained OC component. Mixed OC and Bx is the average composition of splits b3 and b5. "Internal" refers to the irradiation tube number. Concentrations of oxides are given in weight percent and trace elements are in μg/g, except for Au and Ir, which are given in ng/g.

bulk composition similar to that determined by analysis of fused beads (Table 1). The average CaO concentration from FB-EMPA analysis appears to be high because it yields a high molar Ca/Al of 3.5 and results in a higher proportion of high-Ca pyroxene in the normative mineral proportions compared to that inferred from modal recombination. This mismatch is consistent with a contribution of about 0.5 wt.% CaO from calcite deposits (see below). Without this contribution, the bulk OC composition would have a molar Ca/Al of about 3.1, whereas the maximum Ca/Al obtained after modal recombination of observed mineral compositions is about 3.0. This Ca/Al value is still much higher than that calculated from the composition given by Bridges et al. (2002) and from the modal recombination of Fagan et al. (2003) (Table 2). To obtain Al_2O_3 of 5.7 and Ca/Al ~2 requires some 15% plagioclase and 10% high-Ca pyroxene, using our average mineral compositions, and indeed Fagan et al. (2003) reported 14.2% plagioclase and 8.7% high-Ca pyroxene in their mode. The higher values of Ca/Al observed in our subsamples result from low proportions of plagioclase coupled with high proportions of calcic pyroxene.

Table 4. Mineral compositions in NWA773 olivine-cumulate lithology.

	Olivine n = 18	Hypersthene n = 1	Pigeonite n = 7	Augite n = 7	Plagioclase n = 9	K-feldspar n = 3	RE-merrillite n = 1	Cr-spinel n = 6	Ilmenite n = 4
SiO_2	37.4	53.2	53.4	52.2	46.3	60.6	1.04	0.05	0.08
TiO_2	0.02	0.64	0.43	0.72	0.06	0.25	0.04	13.2	54.3
Al_2O_3	0.00	1.04	1.39	2.49	33.5	19.7	0.07	8.49	0.04
Cr_2O_3	0.10	0.36	0.58	0.85	na	na	na	35.1	0.45
FeO	28.6	16.5	15.6	9.15	0.41	0.49	1.81	38.3	39.7
MnO	0.28	0.38	0.29	0.20	0.13	0.06	0.00	0.34	0.46
MgO	33.5	25.5	22.2	17.0	0.12	0.00	4.49	4.31	5.22
CaO	0.17	1.93	5.88	17.5	17.7	0.47	42.1	0.03	0.20
BaO	na	na	na	na	0.01	1.07	na	na	na
Na_2O	<0.01	0.01	0.024	0.04	1.07	0.42	0.59	na	na
K_2O	na	na	na	na	0.36	15.3	0.04	na	na
P_2O_5	na	na	na	na	na	na	43.0	na	na
Oxide Sum	100.0	99.6	99.7	100.1	99.7	98.3	93.2	99.8	100.5
Mg/(Mg + Fe)	0.68	0.73	0.72	0.77	0.34		0.82	0.17	0.19
Wo/An		3.8	12.0	36.2	88.2				

"na" = not analyzed; "nd" = not detected; Mg/(Mg + Fe) = molar. Wo/An = wollastonite content (pyroxene) and anorthite content (plagioclase). For plagioclase, the An content ranges from 93.8 to 80.5. Oxide sum for RE-merrillite is absent some 5.7 wt% RE_2O_3 (see table 7). Spinel includes 0.47 wt% V_2O_3.

Both the Bx and OC lithologies have low TiO_2 concentrations. In subsamples analyzed by FB-EMPA, we obtain average concentrations of 0.78±0.08 and 0.24±0.06 wt.% for Bx and OC, respectively. These compare to values of 0.84±0.05 and 0.4 wt.% for the breccia and olivine gabbro, respectively, determined by Fagan et al. (2003) and 0.4 wt.% for the olivine cumulate determined by Bridges et al. (2002). Even after "correcting" the Bx composition for a reasonable OC clast content (i.e., 15%, Section 5), the bulk TiO_2 concentration of Bx is only ~0.88 wt.%. For a mafic volcanic breccia, this TiO_2 concentration of <1 wt.% places the NWA773 breccia, by definition, into the very-low-TiO_2 (VLT) category.

4.3. Textures

The texture of the olivine cumulate lithology is clearly igneous and the distribution and occurrence of minerals indicate that the lithology is orthocumulus. Olivine and pigeonite primocrysts form the coarsest grains, typically hundreds of μm to over a mm for some grains. In our sections, the largest olivine primocryst is 1×1.5 mm and euhedral, and one olivine glomerocryst is 1.5×2 mm in cross section, consisting of several subhedral olivine crystals (Fig. 3). Augite and plagioclase form smaller grains that generally conform to irregular intercumulus spaces left among the coarser grains and thus represent crystallization products of intercumulus melt (especially Fig. 3). In some cases, plagioclase and pyroxene surround olivine. The main silicate paragenesis is olivine → olivine + pigeonite → pigeonite + augite → pigeonite + augite + plagioclase, similar to many lunar mare basalts (Bence and Papike, 1972). This crystallization sequence is the same as that reported by Fagan et al. (2003). Minor occurrence of low-Ca orthopyroxene appears to be late (see section 6). The Mg/Fe ratios of the mafic silicates indicate equilibration of Fe and Mg ($Mg'_{Aug} > Mg'_{Opx} > Mg'Pig > Mg'Ol$, Table 4); however, plagioclase retains compositional variations (normal zoning) consistent with intercumulus crystallization (see section 6). Because of the retention of some normal igneous zoning and a significant proportion of trapped intercumulus melt, we consider this lithology to be an *orthocumulate* as opposed to an *adcumulate* or *heteradcumulate*.

Exsolution lamellae in pyroxene are resolved at the micrometer scale in backscattered-electron and X-ray images of the pigeonite grains, but not augite (e.g., Fig. 5). Two of the pyroxene grains analyzed with the ion probe, IP1 and IP7, have discernable thin (~1 μm) lamellae of high-Ca pyroxene, spaced about 2.5–4 μm apart, in pigeonite hosts, and the pigeonite is not inverted. In two of the more calcic pigeonite grains, IP4 and IP5, exsolution lamellae are just barely visible in Ca X-ray images, with high-Ca (augite) and low-Ca (pigeonite) lamellae of subequal width. Because some of the pigeonite grains are exsolved, care was taken to ensure that both the IMP and EMP analyses provide a representative composition and integration of lamellae. The Ca concentrations measured by EMP correlate well with those measured by IMP, assuring that the pyroxene compositions measured by the two methods correspond. This issue is especially important because we use the wollastonite content of pyroxene to calculate distribution coefficients for the REE (McKay et al., 1986). In one case for pyroxene analyses (IP Px 6, low-Ca) and in the two olivine analyses, Ca by IMP exceeds that measured by EMPA; these are discussed in section 5.

Among the accessory minerals in OC, chromian spinel ($Sp_{12}Ch_{46}Pi_5Ul_{37}$) forms small, equant grains, ~100 μm or less in size. Spinel grains typically occur within olivine grains or between olivine and pigeonite grains. Ilmenite grains are elongate and small, typically <150 μm in length, and they occur in intercumulus areas with pyroxene, K-feldspar, RE-merrillite, and troilite–Fe-Ni metal intergrowths. Ilmenite grains contain about 5% MgO. Oxide compositions do not vary significantly and average compositions of spinel and ilmenite are listed in Table 4. Metal grains occur in very small masses with troilite and are Ni-rich (55.5 wt.% Ni, 40.9% Fe, 1.5% Co, <0.03% P). The most sodic plagioclase, K-feldspar, ilmenite, RE-merrillite, troilite, and Fe-Ni metal appear to represent

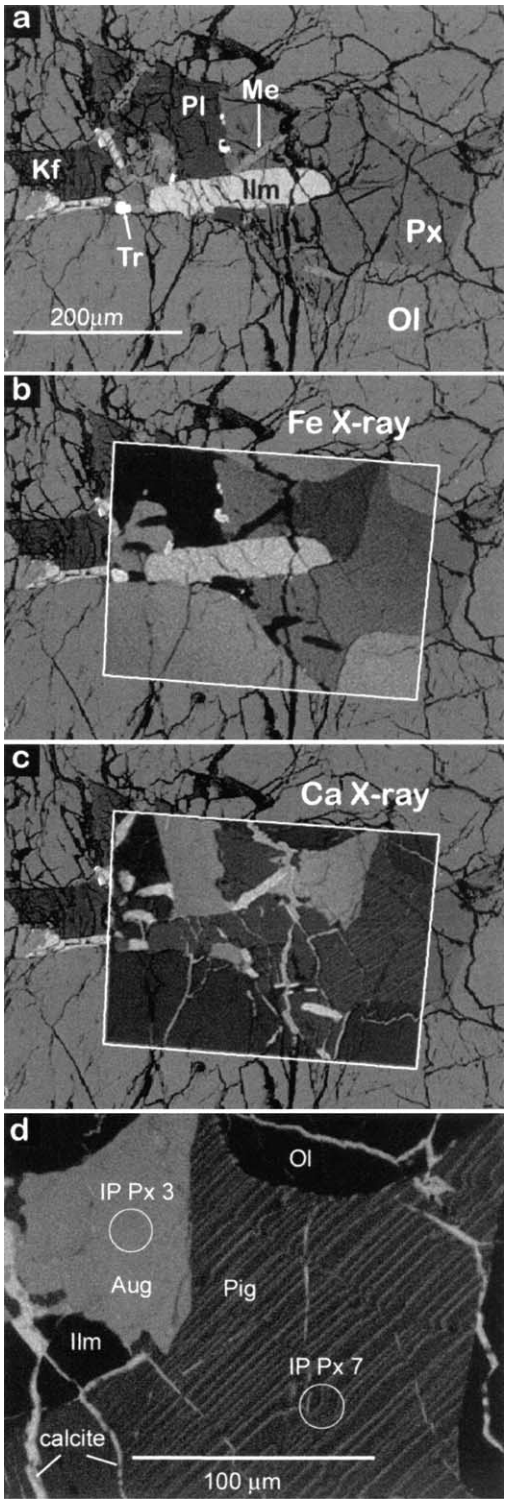

Fig. 5. Intercumulus area representing solidified trapped melt in OC. (a) BSE: Ol – olivine, Px – pyroxene, Pl – plagioclase, Ilm – ilmenite, Kf – K-feldspar, Me – RE-merrillite, Sp – spinel, Tr – troilite; (b) BSE with Fe X-ray image overlay; (b) BSE with Ca X-ray image overlay; (d) close-up Ca X-ray image of pyroxene area showing location of IP Px3 and IP Px7 spots. Augite and pigeonite are difficult to tell apart in BSE, but are readily distinguished in the Ca X-ray image. Calcite is bright in the Ca X-ray image and fills fractures; RE-merrillite is almost as bright, but forms small bladed crystals that are black in the Fe X-ray image.

late-stage trapped melt, and the sulfide-metal grains may represent a very-late-stage immiscible-liquid separation (Dymek et al., 1975).

All fragments and the polished sections of NWA773 that we have observed contain evidence of terrestrial alteration. Abundant Ca-carbonate deposits occur on surfaces of broken fragments that expose calcite-rich fracture fillings (Fig. 1). Calcium X-ray images show that calcite occurs within fractures, which range from several micrometers to tens of micrometers in width, pervasively throughout the interior of the meteorite (Figs. 4f, 5). Energy-dispersive EMP spot analyses of the fracture fillings reveal mostly calcite, but some spots show evidence of silica and phosphorus, and some Al-bearing silicates in phases too small to resolve by EMP analysis. Fagan et al. (2003) also report sulfates in fractures.

Despite the reddish surface coloration evident on many of the fragments, which we interpret to be thin Fe-oxide coatings on grains that were exposed to terrestrial aqueous fluids, silicates lack observable alteration in polished probe mounts, even along fracture boundaries. Calcite forms crusts and deposits in open fractures (Figs. 3, 4f), but we see no evidence for leaching or reaction of minerals grains along fracture surfaces. Lunar RE-merrillite and matrix glass, as well as Fe-Ni metal, also remain intact and unaltered, although the high Ni content of the metal probably helps to stabilize it (Foley et al., 1955). Potential effects of terrestrial alteration are discussed in section 7.

5. BULK TRACE-ELEMENT COMPOSITIONS

Both lithologies of NWA773 have a trace-element signature that is unusual for a VLT major-element composition in comparison to other lunar volcanic rocks. The unusual coupling of very low Ti and relative incompatible-element enrichment is illustrated in Figure 6a (Ti vs. Th) for lunar mare basalts and basaltic meteorites. The cumulate and breccia-matrix lithologies of NWA773 have over 1.5 to 2 times the Th, U, and K concentrations of other VLT basalts. Both the breccia and the cumulate are relatively enriched in LREE compared to HREE and are more depleted in Eu than most other known lunar volcanic rocks (Table 3, Fig. 6b). The absolute concentrations of incompatible trace elements are not unusually high for lunar rocks in general, with concentration levels at about 0.08 × and 0.13 × KREEP (as defined for mafic impact-melt breccias, e.g., Warren, 1988; Jolliff, 1998), respectively for OC and Bx, but they are remarkably high compared to other Ti-poor mare rocks, and the LREE/HREE values equal or slightly exceed those of KREEP (e.g., La/Yb=3.5 compared to 3.2 for KREEP; Fig. 7).

The NWA773 lithologies have relatively low Sc concentrations (37 μg/g in Bx and 22 μg/g in OC) compared to most lunar volcanic rocks, again, typical of VLT basalt compositions (Fig. 8). The composition of OC can be understood in terms of its mineral assemblage, especially its high olivine content, relative to Bx. One subsample (INAA) has relatively high CaO (a9) and although we noted a coarse plagioclase clast in this fragment, it appears to be the Ca-carbonate content that mainly causes high CaO because Eu is not similarly enriched (Fig. 8b). The Bx lithology composition is displaced toward olivine with respect to common correlations observed among mare basalts, such as FeO vs. CaO and FeO+MgO vs. Al_2O_3. Subtraction of

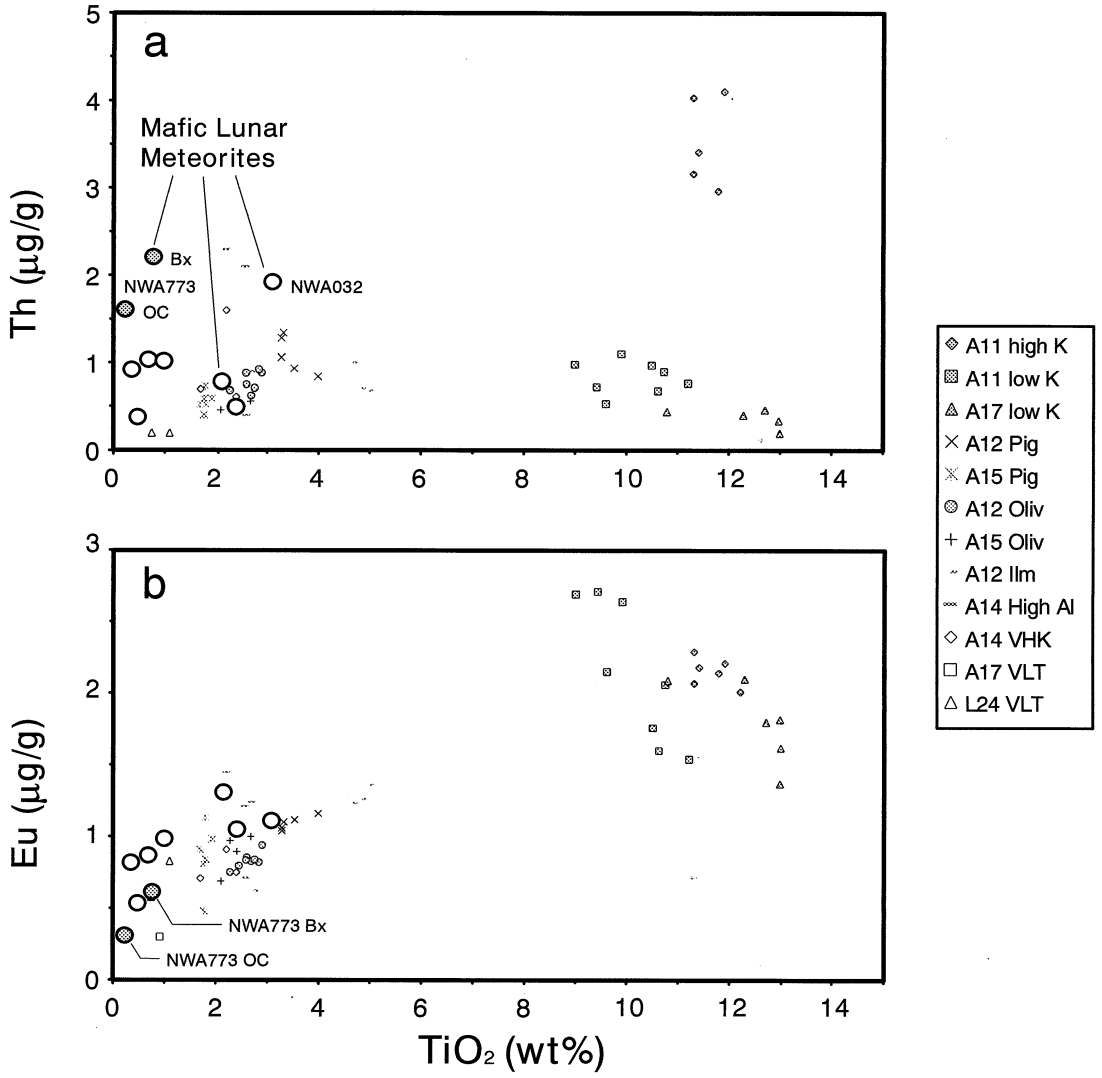

Fig. 6. (a) Ti-Th and (b) Ti-Eu for mare basalts and mafic lunar meteorites. NWA773 components have high Th concentrations for their low-Ti compositions and they have among the lowest Eu concentrations of all mare basalts and mafic lunar meteorites.

some 15% of OC from the Bx composition yields an estimate (Bx′) of the composition of the breccia components minus small OC clast components that is more in line with other lunar volcanic rocks. Although the choice of 15% is somewhat arbitrary, it is useful to make this calculation to assess the origin of the Bx component. For Sc, this subtraction yields 40 μg/g for the Bx′ component (Table 3). Using data from splits analyzed by INAA, we obtain 17.8 wt.% FeO and 12.3 wt.% CaO for this composition compared to 17.2 and 11.6 wt.%, respectively, from fused-bead data. This composition is ferroan, with molar Mg/(Mg+Fe) = 0.53, consistent with the relatively evolved basaltic assemblages as shown in Figure 4. This composition has about 0.14 × average impact-melt-breccia KREEP concentrations of the REE and exactly the same La/Yb as the KREEP composition.

The OC lithology has a high Ni concentration of 236 μg/g, which is no doubt related to the abundance of olivine (our IMP analysis of Ni in olivine yielded 318 μg/g). OC also has a relatively high Co concentration of 92 μg/g. By comparison, the 72415 dunite from Apollo 17 has 160 μg/g Ni and 55 μg/g Co (Laul and Schmitt, 1973). A bulk Ni/Co value of 2.4 and Ir concentrations below our detection level (<4 ppb, Table 3) are consistent with lunar indigenous Ni, not meteoritic contamination. Ni-rich metal in OC (55 wt.% Ni) also occurs in dunites such as 72415 (up to 33 wt.% Ni; Dymek et al., 1975).

6. MINERAL COMPOSITIONS

6.1. Major- and Minor-Element Compositions of OC Silicates

As discussed in section 4, the pyroxene grains in OC in the sections we have examined appear to be fairly well equilibrated in terms of Mg/(Mg+Fe), and individual grains are compositionally uniform aside from fine exsolution (*Mg′,Hyp:* 74; *Mg′,Pig:* 72–74; *Mg′,Aug:* 75–80). Different pyroxene grains,

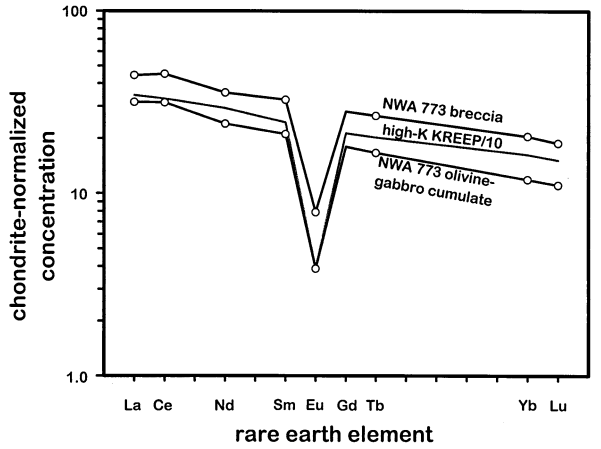

Fig. 7. Chondrite-normalized REE patterns of NWA773 breccia and olivine cumulate. Pattern of average high-K KREEP (Warren; 1988) divided by 10 shown for comparison. NWA773 patterns are subparallel to that of KREEP with the exception of an apparent slightly positive Ce anomaly. Note, however, that uncertainties on Nd are typically 10–15% compared to 1–2% for La, Ce, and Sm. Values for normalization are for C1 chondrites (Anders and Grevesse, 1989) × 1.36, which gives Sm_{C1} = 0.2 μg/g. Gd value is interpolated between Tb and Sm.

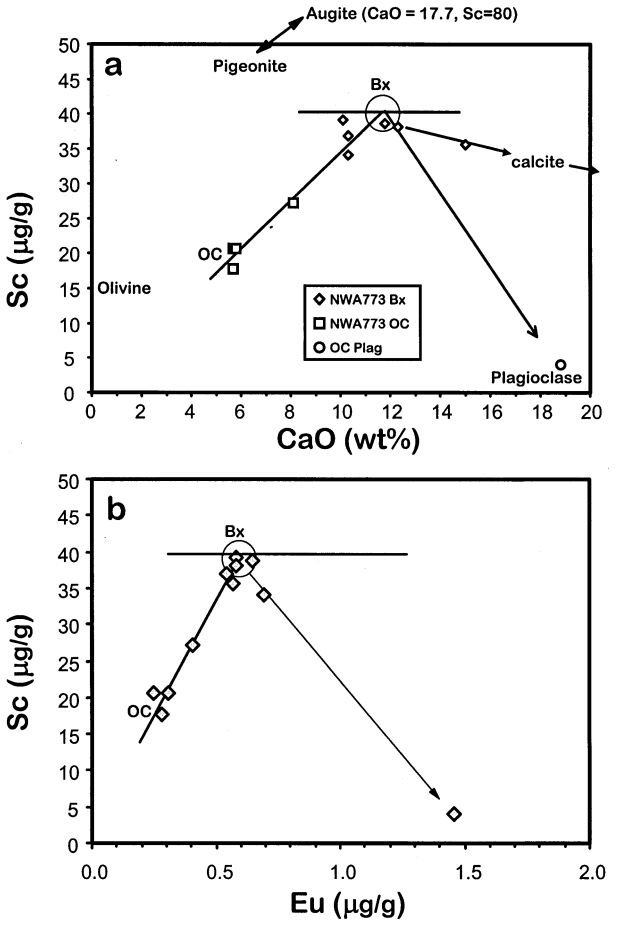

Fig. 8. Concentrations of (a) Sc vs. CaO and (b) Sc vs. Eu in splits of NWA773 analyzed by INAA. In part (a), the circle marks the inferred composition of the BX matrix at about 40 μg/g Sc. The high CaO subsample appears to be rich in calcite, not plagioclase, as further indicated by the fact that in terms of Sc-Eu, it lies on the OC-Bx mixing line.

however, display variations in "bulk" Ca content. Pyroxene compositions in OC cluster along tielines between augite, pigeonite, and low-Ca orthopyroxene in the pyroxene quadrilateral (Fig. 9). For the compositions shown in the figure, bulk Wo contents of pigeonite range from 8 to 16% and augite, 34–38% (Table 5), indicating crystallization through the ~1200–1050°C interval (Fig. 9) for individual grains. Fagan et al. (2003) analyzed more grains and found a larger range of *Mg′* values for pigeonite (~70–76), but about the same range of Wo contents. Fagan et al. (2003) also showed several low-Ca pyroxene analyses at ~ Wo_3 (their Fig. 4). The three pyroxene types, pigeonite, augite, and orthopyroxene, appear to have coexisted around 1060°C (Fig. 9), but the melt composition was calcic enough that little orthopyroxene formed. Exsolution compositions suggest that equilibration in terms of Ca did not occur much below ~1020–1050°C. Variations in Ti/Al in pyroxene grains indicate early formation of calcic pigeonite and augite [Ti/Al (atomic) <0.25 for IP 2, IP 3, IP 4, and IP 5], before the onset of plagioclase crystallization, whereas the highest Ca augite (#189, Fig. 9) and orthopyroxene (IP 6, Fig. 9) have Ti/Al of 0.42 and 0.44, respectively, indicating later crystallization, after plagioclase saturation (Bence and Papike, 1972). Variations in Ti/(Ti+Cr) correlate with Ti/Al (Table 5), consistent with the inferred crystallization sequence. Fagan et al. (2003) reported the same minor-element systematics for pigeonite and augite in the olivine gabbro and also interpreted the variations to reflect the crystallization sequence. Pigeonite grain IP 1 (Table 5, Fig. 9), however, which is exsolved on a micrometer scale, has relatively low Ca, yet has low Ti/Al, indicating early crystallization.

Olivine grains in OC range in Mg/(Mg+Fe) from 0.64 to 0.70, but most are in the range 0.67–0.68 (e.g., Table 3, Table 6), consistent with the mean reported by Fagan et al. (2003). Concentrations of CaO in olivine in OC range from 0.11 to 0.34 wt.% and average 0.17. In the large olivine grain shown in Fig. 3 (bottom), CaO varies from 0.34 wt.% near the center to 0.16 wt.% at the rim. These values are somewhat high compared to intrusive, igneous lunar olivine, which is generally <0.13 wt.%, and at the low end for olivine in lunar basalts (Ryder, 1992; Papike et al., 1998: Tables A5.8, A5.10). Fe/Mn values average ~100+/−10, which is typical of lunar olivine (Papike, 1998; Karner et al., 2003).

Plagioclase grains in OC retain zoning, ranging in An content from 94 to 80 (Table 7). The highest An values occur in cores of grains and the most sodic values occur at rims adjacent to intercumulus assemblages of K-feldspar, ilmenite, RE-merrillite, troilite, and Fe-Ni metal. Retention of compositional variations in plagioclase despite Fe-Mg equilibration in mafic silicates is not surprising because the coupled substitution of Na+Si↔Al+Ca requires a more difficult structural modification than Fe↔Mg exchange in pyroxene and olivine (Morse, 1984). Concentrations of ~0.4–0.8 wt.% MgO+FeO in plagioclase are high for lunar intrusive rocks, but are in the low part of the range typical of plagioclase in lunar basalts (e.g., Papike et al., 1998). K-feldspar grains occur in intercumulus assemblages and compositions include BaO ~0.7–1.7 wt.%. In

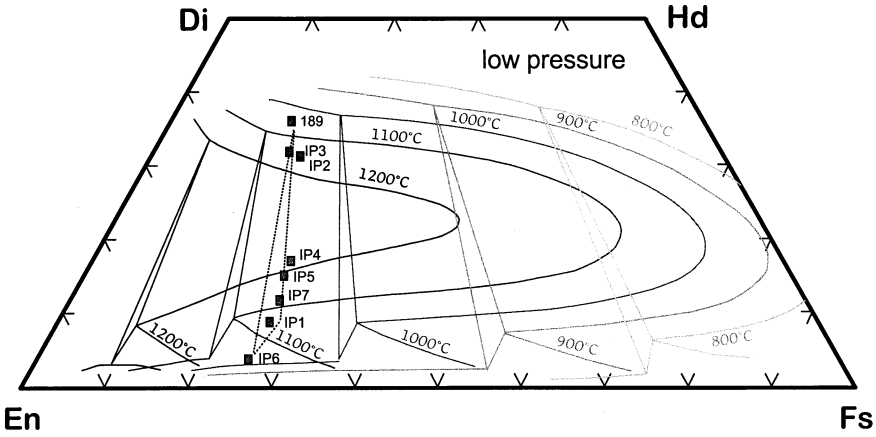

Fig. 9. Compositions of pyroxene grains in OC projected onto quadrilateral isotherms (Sack and Ghiorso, 1994) with Wo contents corrected for non-quadrilateral components. Only the compositions where ion probe analyses were taken are shown here plus one analysis that shows the Ca-rich extent of measured augite grains (189, 10 μm spot). "IP" electron microprobe analyses were done with 30 μm spot size to cover an equivalent mixture of high- and low-Ca lamellae as the ion microprobe spots where lamellae were present to obtain a representative "bulk" pyroxene analysis for each grain. Variations in Ca contents suggest a crystallization interval from ~1200–1050°C. The dashed tielines indicate stable coexisting pigeonite-augite-orthopyroxene compositions at about 1060°C.

the Bx lithology, one coarse (~2 mm) plagioclase clast of basalt/gabbro affinity (An_{95}, 0.48% FeO, 0.19% MgO; Fig. 4a) occurs in subsample a1. Although this plagioclase grain could simply be a fragment of coarse-grained gabbro, it is coarser than any plagioclase seen in our sections of the cumulate lithology or reported by Fagan et al. (2003), and it contains an inclusion of pigeonite that is more ferroan (Mg/(Mg+Fe = 0.64) than observed in OC. The presence of this coarse grain and its composition might suggest the possibility that plagioclase accumulation complementary to OC occurred somewhere in the target area of the impact that produced NWA773; however, we observed no polycrystalline plagioclase lithic clasts in probe mounts nor were any of the splits analyzed by INAA or as fused beads dominated by plagioclase.

6.2. Trace-Element Compositions of OC Silicates and Merrillite

The relatively REE-rich bulk composition of the NWA773 olivine cumulate is reflected in the REE concentrations and patterns of its silicates and merrillite. Concentrations of REE (and Sc, Cr, and Al) in pyroxene vary according to Wo content, with concentrations higher in augite than in pigeonite (Fig. 10). Concentrations of REE, however, also vary within these groups over about a factor of 2–3 (Table 5, Fig. 11). Of the pyroxenes, the augite grains have the highest La/Yb values, consistent with distribution coefficients (McKay et al., 1986). The normalized REE pattern of one of the pigeonite grains (IP 7) has a significant positive-Ce anomaly. The analysis of a low-Ca grain, IP 6, has a fairly steep HREE slope, typical for orthopyroxene, but an unusually flat LREE slope (i.e., La-enriched compared to expected pattern) and high overall REE concentrations relative to pigeonite considering its low Ca content. One possible reason for the relatively high REE concentrations of IP 6 is that it formed late, which is consistent with high Ti/Al and having crystallized at the lowest temperature (Fig. 9). The REE concentrations of pigeonite grains IP 4, IP 5, and IP 7 increase with the crystallization sequence inferred from pyroxene thermometry (Fig. 9) and minor element variations, e.g., Ti/(Ti+Cr). As mentioned above, however, IP 1, which has the lowest Wo content (8.1, Table 5), has low REE concentrations, consistent with low Ti/Al and inferred early crystallization. The apparent relative LREE enrichment of IP6 and the Ce anomaly of IP7 may be related to terrestrial contamination, as discussed below. All pyroxene REE patterns have deep negative Eu anomalies.

Olivine REE concentrations are generally low and chondrite-normalized patterns slope upward toward Yb and Lu, typical of olivine (Fig. 12, Table 6). One pattern, however, shows anomalous LREE enrichment, which we attribute to terrestrial contamination as discussed in the next section. Other elements expected to be at extremely low concentrations in olivine, such as Sr and Ba (McKay and Weill, 1976), correlate with La and are probably also terrestrial contaminants. Concentrations of Ni and Co, measured by IMP, are 318 μg/g and 250 μg/g, respectively, consistent with elevated concentrations of Ni and Co in the bulk splits analyzed by INAA. These values are in the range that is typical for olivine-rich lunar basalts and picritic volcanic glasses (Papike et al., 1998).

Feldspar REE concentrations are listed in Table 7 and shown in Figure 13. We measured only one plagioclase grain, including its calcic (An_{94}) core and its more sodic (An_{85}) rim, and one K-feldspar grain. In the plagioclase grain, the REE concentrations vary according to Ab content, with the more sodic rim composition having about a twofold to threefold enrichment, consistent with the rim having formed from late-stage trapped melt. The Eu concentrations of the two plagioclase analyses are 1.5 μg/g and 2.5 μg/g for the calcic core and sodic rim, respectively. These values are not unusually low for basaltic plagioclase, judging by bulk Eu concentrations, and result in positive Eu anomalies typical of lunar plagioclase. The bulk Eu concentrations of NWA773 OC and Bx (0.29 and 0.60 μg/g) are low because these lithologies are plagioclase poor, espe-

Table 5. Pyroxene compositions, NWA773 olivine cumulate.

	IP 1 Pig	IP 4 Pig	IP 5 Pig	IP 7 Pig	IP 2 Aug	IP 3 Aug	IP 6 Hyp
			major elements, wt.% (electron microprobe)				
SiO_2	53.91	53.00	53.28	53.59	52.00	52.25	53.03
TiO_2	0.20	0.35	0.36	0.60	0.81	0.70	0.55
Al_2O_3	0.89	1.86	1.65	0.96	2.19	2.58	0.81
Cr_2O_3	0.43	0.79	0.77	0.37	0.84	0.85	0.33
FeO	16.45	15.10	15.30	16.25	10.18	8.80	16.59
MnO	0.28	0.32	0.25	0.34	0.28	0.17	0.31
MgO	23.80	20.75	21.43	22.42	17.00	16.95	26.19
CaO	4.04	7.89	6.75	4.74	16.81	17.68	1.94
Na_2O	0.02	0.01	0.04	0.02	0.05	0.04	0.01
Total	100.03	100.07	99.83	99.29	100.16	100.02	99.75
			cation ratios (based on 6 oxygen atoms per formula unit)				
Mg/(Fe+Mg)	0.72	0.71	0.71	0.71	0.75	0.77	0.74
Ti/Al	0.14	0.12	0.14	0.40	0.24	0.17	0.43
Ti/(Cr+Al)	0.31	0.30	0.31	0.61	0.48	0.44	0.62
Wo[a]	8.1	16.2	13.9	9.7	34.7	36.7	3.8
En	66.2	59.5	61.5	64.2	48.9	49.0	71.0
Fs	25.7	24.3	24.6	26.1	16.4	14.3	25.2
			trace elements, μg/g (ion microprobe)				
K[b]	13	26	30	59	14	19	69
Sc	32	54	56	41	75	87	41
V	81	169	162	90	223	157	62
Sr[b]	0.6	2.6	2.5	7.1	4.2	5.1	9.1
Y	11.2	17.1	22.0	27.3	51.9	126	18.1
Ba[b]	0.7	3.6	2.1	9.4	0.9	6.5	9.6
La	0.14	0.21	0.50	0.33	1.42	3.87	0.57
Ce	0.77	1.13	2.51	2.18	7.04	19.6	1.58
Pr	0.21	0.19	0.51	0.22	1.80	3.77	0.25
Nd	1.06	1.68	2.74	1.48	9.21	25.7	1.30
Sm	0.44	0.59	1.08	0.84	3.66	9.98	0.53
Eu	0.02	0.02	<0.01	<0.01	0.06	0.12	0.01
Gd	0.59	1.19	1.62	1.68	6.72	14.3	0.84
Tb	0.15	0.31	0.38	0.41	1.12	2.36	0.24
Dy	1.38	2.77	3.04	3.14	8.45	18.7	2.26
Ho	0.27	0.50	0.70	0.78	1.69	4.01	0.54
Er	0.97	1.75	2.13	2.75	4.76	11.3	2.25
Tm	0.17	0.20	0.40	0.39	0.66	1.09	0.43
Yb	1.02	1.41	1.94	2.86	3.77	7.61	3.39
Lu	0.16	0.25	0.17	0.48	0.41	0.88	0.57

[a] Wo (wollastonite), En (enstatite), and Fs (ferrosilite) contents calculated for EMP analyses corresponding to IMP spots.
[b] K, Sr, Ba reported here as indicators of terrestrial contamination.
Mg/(Mg + Fe) calculated from cation proportions (EMP).
Typical uncertainties for the REE (1-sigma, counting statistics, in %): Y, 3; La, 10; Ce, 7; Pr, 9; Nd, 5; Sm, 10; Eu, 70; Gd, 10; Tb, 12; Dy, 5; Ho, 9; Er, 5; Tm, 11; Yb, 8; Lu, 17.

cially our sample of OC. Fagan et al. (2003) reported 0.35 μg/g for the olivine gabbro, but their mode for this lithology also contained more plagioclase than ours. The REE concentrations of the K-feldspar grain that we analyzed are extremely low, so we report only the LREE La through Nd in Table 7. Several of the REE have severe interferences from Ba oxides, and possibly also from LREE monoxides, that are not resolved in our analysis or that lead to unacceptably high uncertainties. The concentration of Y, taken as a proxy for the HREE, is extremely low ($<0.25 \times$ chondritic value), reflecting very low concentrations of the HREE in K-feldspar and very low K-feldspar/melt partition coefficients.

Merrillite in NWA773 OC is REE-rich, as it is in all other lunar rock types that contain it; concentrations range from 2000 (Lu) to 11,000 (La) times chondrites and ~17 μg/g Eu (Table 6, Fig. 14). Its La/Yb value of ~5 is high compared to KREEP (~3.2). In OC, RE-merrillite grains are very fine grained (e.g., 8–10 μm wide and 30–50 μm long) and represent the end-stage uptake of REE from residual, trapped melt. OC RE-merrillite is relatively Sc rich, with 63 μg/g, and its Mg' is 82, consistent with the expected distribution of Fe and Mg relative to the coexisting mafic-silicate compositions (Hess et al., 1990; Jolliff et al., 1993). Thorium is also enriched in RE-merrillite, with a concentration of over 1000 μg/g.

7. DISCUSSION

7.1. Terrestrial Contamination

We begin the discussion with an assessment of the effects of terrestrial contamination because several of the key features of NWA773 relate to its chemical composition. It must be shown that the unusual features that might be attributed to lunar sources or process are not somehow a result of terrestrial alteration. Chief among these features is the enrichment in Sr and Ba, and high LREE/HREE. Calcite deposits are the most

Table 6. Compositions of olivine and RE-merrillite in NWA773 OC lithology.

	Olivine 1	Olivine 2	RE Merrillite
	major elements, wt% (electron microprobe)		
SiO_2	37.50	37.88	1.00
TiO_2	0.04	0.06	0.04
Al_2O_3	0.00	0.00	0.07
Cr_2O_3	0.05	0.11	na
FeO	28.75	28.16	1.81
MnO	0.28	0.13[b]	<0.03
MgO	33.62	33.75	4.50
CaO	0.18	0.14	42.10
Na_2O	<0.01	<0.01	0.60
P_2O_5	na	na	43.00
Oxide Sum[a]	100.4	100.2	93.1
Mg/(Mg+Fe)	0.68	0.68	0.82

	trace element concentrations (ion microprobe)					
	μg/g	+/−	μg/g	+/−	μg/g	+/−
Sc	20	0.4	17	0.5	68	2
V	13	0.4	12	0.6	7	1
Ni	na		318	13	na	
Co	264	4	251	6	na	
Sr	0.10	0.02	3.49	0.4	184	5
Y	1.74	0.095	0.705	0.278	20192	52
Ba	0.06	0.01	7.1	0.2	41	6
La	<0.04	0.009	0.138	0.479	3637	27
Ce	nd	0.003	0.257	0.038	9249	49
Pr	<0.006	0.003	0.016	0.031	1172	15
Nd	<0.009	0.006	0.061	0.010	5179	41
Sm	nd		nd		1378	32
Eu	<0.02	0.002	<0.02	0.020	16.9	2.4
Gd	0.014	0.007	0.011	0.009	1379	37
Tb	0.011	0.004	0.011	0.019	329	10
Dy	0.098	0.015	0.040	0.007	2152	27
Ho	0.055	0.009	0.016	0.017	421	11
Er	0.230	0.022	0.102	0.008	1116	20
Tm	0.046	0.009	0.027	0.024	140	6
Yb	0.504	0.047	0.192	0.010	683	20
Lu	0.144	0.017	0.049	0.046	66	7

Errors shown for trace elements are 1-sigma, from counting statistics.

na = not analyzed; nd = not detected.

[a] RE oxides contribute 5.7 wt.% to the merrillite oxide total.

[b] MnO in Olivine 2 is atypically low (see Table 3).

Table 7. Compositions of feldspars in NWA773 OC lithology.

	Plagioclase core	Plagioclase rim	K-feldspar
	major elements, wt% (electron microprobe)		
SiO_2	45.20	46.69	60.57
Al_2O_3	34.65	33.26	19.7
FeO	0.29	0.32	0.49
MgO	0.11	0.15	<0.02
CaO	18.83	17.35	0.47
BaO	0.008	0.026	1.07
Na_2O	0.59	1.20	0.42
K_2O	0.15	0.45	15.32
Total	99.81	99.44	98.04
An	93.8	85.2	2.4
Ab	5.3	11.8	3.8
Or	0.9	3.0	91.8
Cn	0.01	0.05	2.0

	trace element concentrations (ion microprobe)					
	μg/g	+/−	μg/g	+/−	μg/g	+/−
Sr	105	2	132	2	83	2
Y	1.44	0.07	2.38	0.17	0.47	0.04
La	1.74	0.10	6.02	0.44	2.58	0.19
Ce	4.18	0.20	12.26	0.77	1.15	0.09
Pr	0.47	0.03	1.52	0.12	0.07	0.02
Nd	1.86	0.07	4.94	0.22	0.15	0.04
Sm	0.35	0.06	0.88	0.12	ui	
Eu	1.46	0.09	2.57	0.22	ui	
Gd	0.27	0.05	0.81	0.15	bd	
Tb	0.04	0.01	0.10	0.03	bd	
Dy	0.21	0.02	0.39	0.05	ui	
Ho	0.06	0.01	0.13	0.02	ui	
Er	0.14	0.02	0.16	0.04	ui	
Tm	<0.02	0.01	<0.02	0.02	ui	
Yb	0.04	0.02	0.17	0.05	<0.02	0.02
Lu	0.004	0.006	0.003	0.012	ui	

Errors are 1-sigma, from counting statistics.

ui = unresolved interference; bd = below detection.

An (anorthite), Ab (albite), Or (orthoclase), and Cn (celsian) components calculated from EMP analyses corresponding to IMP spots.

petrographically obvious alteration and they occur throughout the meteorite in the form of fracture fillings. We do not expect the calcite deposits to contain significant REE concentrations. Minor amounts of REE-bearing terrestrial minerals with patterns typical of terrestrial sediments, such as hydrous phyllosilicate clays, could occur in fractures, although we have not observed them. To test for the compositional effects of fracture-filling deposits, we compared the compositions (by IMP) of silicates that appeared to be unaltered to compositions obtained where prominent fractures were intersected by the ion beam. In the case of olivine and at least one low-Ca pyroxene grain, the effects of terrestrial alteration are evident, as discussed in the following paragraphs.

Unusual Ce concentrations relative to La and Nd have been interpreted in previous studies (e.g., Floss and Crozaz, 1991; Crozaz and Wadhwa, 2001; Floss and Crozaz, 2001) to reflect interaction with aqueous fluids and oxidation of Ce^{3+} to Ce^{4+} and subsequent loss or gain, producing a "Ce anomaly." In the REE patterns of OC silicates and RE-merrillite, a general lack of Ce anomaly indicates a lack of alteration. An exception in our data is IP 7 pigeonite (Fig. 5), which has a notably positive Ce anomaly. The IMP spot analysis of this grain crosses a thin carbonate fracture filling, suggesting the possible addition of Ce^{4+} along with calcite (although not necessarily incorporated in calcite) where terrestrial water, probably through repeated

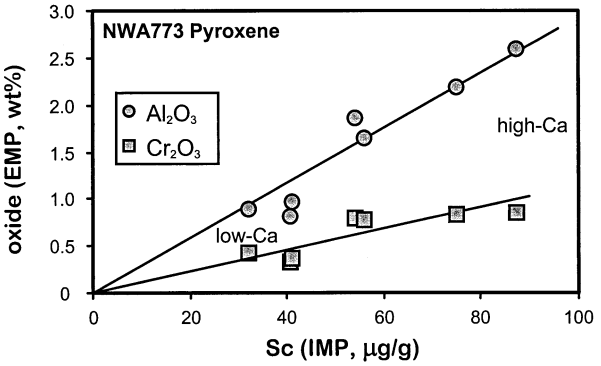

Fig. 10. Sc concentrations vs. Al_2O_3 and Cr_2O_3 in NWA773 OC pyroxene. Lines are visual fits to show positive correlations.

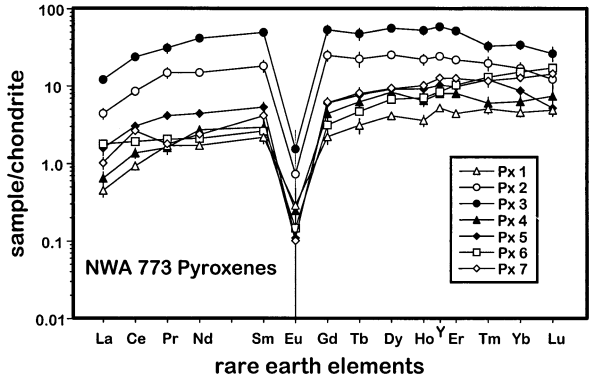

Fig. 11. REE patterns of pyroxene grains in NWA773 normalized to chondrites (Anders and Grevesse, 1989, times 1.36). Two highest patterns are of augite grains. The others are pigeonite except for Px 6, which is orthopyroxene. Px 6 has a steeper HREE slope than the pigeonite grains, but it has a relatively flat LREE slope. When divided by mineral/melt distribution coefficients, the resulting pattern, presumably reflecting that of melt in equilibrium with this grain, is strongly enriched (HREE: 140–160 × chondrite and LREE: 170 (Sm) to 1800 (La) × chondrite). This degree of LREE enrichment in melt, however, is unreasonable, even if this grain crystallized from late-stage trapped melt, so we interpret the relative LREE enrichment of Px 6 to be associated with terrestrial contamination. The pattern of Px 7 has a markedly positive Ce anomaly, also interpreted to result from terrestrial contamination (e.g., Floss and Crozaz, 1991). We plot Y chondrite-normalized values between Ho and Er as a check. Error bars represent uncertainties based only on counting statistics.

wetting and evaporation, as in the formation of caliche, interacted with the meteorite along fractures. The bulk meteorite does have a very slight positive Ce anomaly compared to the other LREE (Fig. 8); however, this feature may be attributable to a relative depletion in La and may not necessarily result from terrestrial weathering, as discussed by Tanimizu and Tanaka (2002) and Korotev et al. (2003).

Slight REE alteration accompanying carbonate deposition in fractures may also account for the LREE enrichment of the olivine grain noted in our data as well as that of Bridges et al. (2002). Carbonate forms sponge-textured deposits in fractures (Fig. 4f) and EDS X-ray analysis shows it to be calcite; however, exceedingly fine-grained material occurs with calcite and shows X-ray peaks for Si and P, which may be associated with trace amounts of material enriched in large-ion-lithophile (LIL) elements typical of terrestrial sediments. In the olivine REE pattern, the inflection in REE concentrations occurs at about Sm or Gd (Fig. 12) and affects all of the larger LREE as well as Ba and Sr. For this reason, the LREE contents of olivine can not be used to assess the REE pattern of the contemporary melt from which olivine in OC accumulated. Correlated variations of Ba and Sr in pyroxene and olivine are probably a result of terrestrial contamination (Fig. 15). The concentrations of the LREE and other LIL elements in olivine, however, are so low, that this level of potential terrestrial contamination does not significantly affect the bulk meteorite composition. If the LIL enrichment noted in our analysis of olivine is typical of contamination associated with vein-carbonate deposition throughout the meteorite, then only about 0.25 μg/g of Ce, for example, less than one percent of the bulk, would have been added by terrestrial weathering.

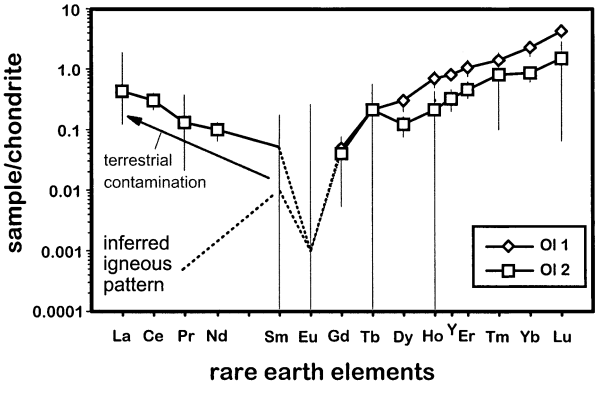

Fig. 12. Chondrite-normalized REE patterns of olivine in NWA773 olivine cumulate. Concentrations measured by IMP, with error bars as shown (no value for Eu). Presumed effect of terrestrial contamination on LREE concentrations is indicated by the arrow and the inferred original igneous olivine REE pattern (before terrestrial contamination) is shown by the dashed line.

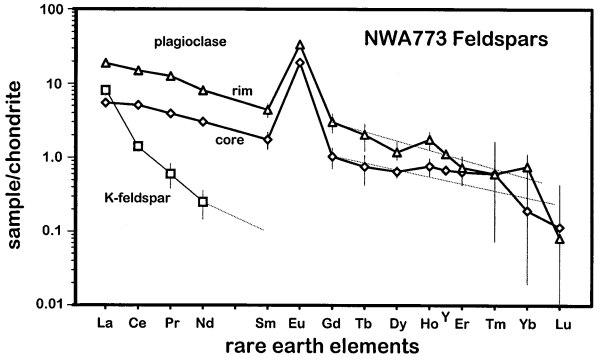

Fig. 13. Chondrite-normalized concentrations of REE in feldspars in NWA773 olivine cumulate. Concentrations measured by IMP. Uncertainties for Tm, Yb, and Lu are large as shown by error bars; light, dashed line for HREE in plagioclase show inferred patterns.

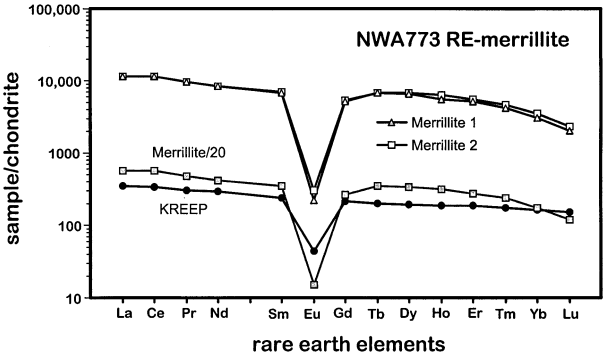

Fig. 14. Chondrite-normalized pattern of RE-merrillite in NWA773 (olivine cumulate lithology). Error bars showing uncertainty on the basis of counting statistics are roughly the size of the symbols. The major-element composition of RE-merrillite 2 (not listed in Table 7) was compromised by overlap onto an adjacent pyroxene grain, but the overlap does not significantly affect the REE pattern or concentrations. Pattern for average RE-merrillite/20 shown for comparison to average high-K KREEP (Warren 1988).

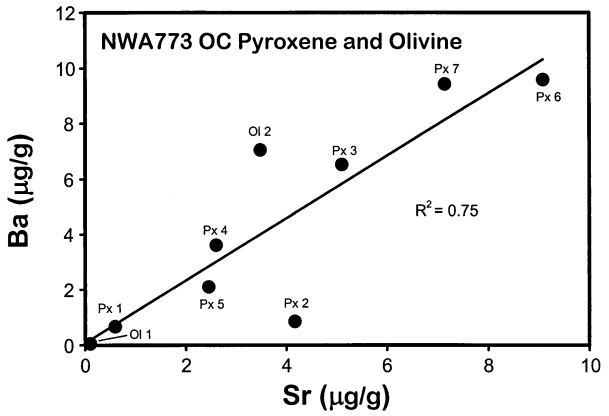

Fig. 15. Ba and Sr concentrations in pyroxene and olivine in NWA773 OC. The correlated variation (linear correlation coefficient = 0.75) is dependent neither on the Ca content of pyroxene nor on whether the mineral is pyroxene or olivine. The enrichment in these elements is attributed to terrestrial contamination. This interpretation is consistent with (1) exceptional LREE enrichment in Ol 2 and Px 6 (orthopyroxene), and (2) a markedly positive Ce anomaly in Px 7 (Fig. 11). In bulk sample splits analyzed by INAA, there is no correlation between Sr and Ba; however, in those splits, Ba and Sr are dominated by feldspars.

Unusual enrichments in some of the elements determined by INAA such as Sr, Ba, Br, or As, which might be attributed to terrestrial weathering (see Korotev et al., 2003), also are not unusually high in the bulk meteorite composition compared to typical lunar materials (Table 3). Furthermore, in the compositions of splits that we initially described macroscopically as possibly altered or containing thin carbonate deposits, there is no evidence that the terrestrial alteration has had any effect on compositions other than slight Ca enrichment. In fact, Br and As are below detection limits in all splits. Concentrations of Ba and Sr are well within the range that is typical for lunar soils. Only one split, a4, is enriched in Ba (335 μg/g) relative to the others (average: 120 μg/g) and this subsample does not have notable carbonate deposits or other evidence of alteration. The subsamples that have the highest LREE/HREE slopes are those that consist mainly of OC, not the ones that appeared macroscopically to have visible evidence of carbonate deposits, oxidation, or sawn faces (Table 3).

Slight enrichments in W and Au may be attributed to contamination during terrestrial residence and from handling and preparation of the sample, e.g., sawing (Korotev et al., 2003).

7.2. Depth of Crystallization of Olivine Cumulate

Silicate mineral compositions in the cumulate lithology are consistent with relatively rapid cooling as would be expected in a shallow intrusive body. The fact that Fe/Mg variation is minimal and that olivine, pigeonite, augite, and orthopyroxene appear to have equilibrium distributions of Fe and Mg (and RE-merrillite, also; cf. Jolliff et al., 1993) indicates that cooling was slower than in extruded mare basalts. Variations in Ca contents in pigeonite and plagioclase grains, however, mean that they did not fully equilibrate and thus they retain a record of crystallization over a significant crystallization interval. CaO concentrations in olivine, although not as high as typically found in lunar basalt olivine, are high compared to concentrations typically found in lunar intrusive rocks. Under slow cooling and equilibrium conditions, Ca is rejected from the olivine structure. Likewise, FeO and MgO contents of plagioclase grains in OC are high relative to most magnesian-suite and ferroan-anorthositic-suite intrusive rocks. Under slow cooling and in well-ordered plagioclase structures equilibrated to low temperatures, these components are rejected and typical FeO+MgO concentrations in slowly cooled or annealed plagioclase are usually less than about 0.3 wt.%.

Pyroxene exsolution textures provide additional evidence for subsurface crystallization, but not very deep. Thin exsolution lamellae in the pigeonite grains and lack of resolvable lamellae in augite indicate relatively rapid cooling and thus, by inference, crystallization in a shallow magma chamber or perhaps a thick, ponded flow. Exsolution lamellae in the pigeonite grains are coarser than commonly observed in coarse-grained mare basalts (where they are rare) and are very narrow compared to plutonic rocks or even to mare-gabbro lithologies in other mafic lunar meteorites, e.g., QUE94281 (Arai and Warren, 1999; Jolliff et al., 1998) and EET87521/96008 (Arai et al., 1996). Equilibration temperatures according to quadrilateral pyroxene thermometry are relatively high, i.e., 1000°C, which is also consistent with relatively rapid cooling.

7.3. Equilibrium Melt of Olivine Cumulate

We define the equilibrium melt of the olivine-gabbro cumulate to be the melt that was in equilibrium with the major-mineral assemblage olivine+pigeonite+augite+plagioclase and that would produce minerals with the observed compositions. The composition of this melt is distinct from that of the *parent* melt of the OC lithology, which we infer had only olivine as a liquidus phase. To estimate the equilibrium melt composition, we used the computer programs of Longhi, Magpox and Magfox (Longhi, 1987, 1991; Longhi and Pan, 1988), which are based on parameterizations of liquidus boundaries and crystal-liquid partition coefficients in the model basaltic system olivine-plagioclase-pyroxene-silica. Through a series of trials constrained to low pressure and approximate mineralogy (olivine, pigeonite, augite, and plagioclase cosaturation) and major mineral compositions, a multiply saturated melt composition was approximated (Table 8, Col. D). We refer to this composition as the "OC equilibrium melt."

To further explore possible compositions that could produce the olivine cumulate (i.e., the *parent* melt), we calculated the effect of adding 40% by mass of olivine to the OC equilibrium melt, using for simplicity the composition of OC cumulus olivine. This melt composition is shown in Table 8, Col. E. It has significantly more alumina than the bulk OC composition because the plagioclase content of the equilibrium melt was constrained to peritectic proportions, i.e., ~33% by mass. The normative plagioclase content of the parent melt composition so calculated is 20% by mass. Using Longhi's equilibrium crystallization program, Magpox, the inferred crystallization sequence for OC (olivine-pigeonite-augite-plagioclase) is obtained with slightly higher SiO_2, e.g., 45 wt.%, and lower Al_2O_3, e.g., 6.5 wt.%, than shown in Table 8. This modification would be consistent with addition of some pigeonite to the 40% added (cumulus) olivine. The predicted crystallization interval

Table 8. NWA773 derivative compositions and comparison to VLT glass and mafic lunar meteorite compositions.

	Lithology Averages										
	Breccia Matrix	Olivine Cumulate	Bx Matrix -15% OC	OC Equil Melt mpox773g′	OC Parent mpox773g′ + 40% Ol	A14 Green Avg A&B	QUE94281 Maf Gls "MG"	QUE94281 Mare YQ1–3	QUE94281 Maf Gls "VLT"	QUE94281 Cryst. VLT model	EET87521 Mare average
	A	B	C	D	E	F	G	H	I	J	K
SiO_2	46.2	44.6	46.5	49.3	44.5	44.6	44.2	44.5	45.7	47.0	48.3
TiO_2	0.78	0.24	0.88	0.94	0.59	0.71	0.41	0.42	0.40	0.80	0.80
Al_2O_3	10.6	3.19	12.0	11.7	7.0	6.9	8.0	9.2	10.6	10.2	12.5
Cr_2O_3	0.40	0.50	0.40	0.26	0.20	0.53	0.72	0.45	0.45	0.36	0.23
FeO	17.3	18.4	17.2	16.8	20.7	20.8	20.0	20.3	18.8	19.0	19.0
MnO	0.26	0.27	0.26	0.25	0.26	0.30	0.23	0.3	0.23	0.28	
MgO	13.2	27.2	10.8	6.63	18.2	17.6	20.0	16.8	13.9	10.8	7.0
CaO	10.8	5.82	11.6	13.7	8.28	8.03	7.2	8.4	9.6	11.0	12.0
Na_2O	0.23	0.13	0.26	0.36	0.22	0.16	0.23	0.3	0.21	0.26	0.38
K_2O	0.10	0.03	0.12	0.05	0.04	0.02	0.02	0.02	0.01	0.05	0.06
P_2O_5	0.09	0.05	0.10	0.06	0.04					0.06	
Sum Oxides	100.1	100.4	100.0	100.1	100.0	99.6	101.0	100.6	99.9	99.8	100.3
Mg/(Mg + Fe)	0.58	0.72	0.53	0.41	0.61	0.60	0.64	0.60	0.57	0.50	0.40
Ca/Al molar	1.84	3.32	1.76	2.12	2.14	2.12	1.63	1.66	1.65	1.96	1.75

Columns A and B are the Bx and OC lithology average compositions; B is an average of our splits b and c (Table 1), Na_2O from INAA (Table 3).

Column C is Bx composition -15% OC [concentration = (Bx-0.15 × OC)/(0.85)].

Column D is a low-P (0.1 Kb) melt composition calculated to be in equilibrium with the OC mineral assemblage [approximated using the program Magpox from J. Longhi (e.g., Longhi and Pan, 1988)].

Column E models the OC parent melt as Col. D + 40% OC olivine. This composition is similar to Apollo 14 green glass types A&B (Col. F; Shearer and Papike, 1993).

Compositions in Cols. F and G are similar to a mafic volcanic glass found in QUE94281 (Col. H), but have distinctively high Ca/Al.

Mafic VLT compositions from QUE94281 and EET87521 lunar meteorites are similar to the Bx matrix -15% OC composition (Col. C) and OC equilibrium melt (Col. D).

G, I, J from Jolliff et al. (1998); H, K from Arai and Warren (1999).

is ~1180–1090°C at low P, and presumably, low-Ca orthopyroxene became stable near the low end of this range.

The major-element composition of the inferred *parent* melt is similar to the VLT volcanic glasses, especially the Apollo 14 green volcanic glass compositions, in particular, those referred to by Delano (1986) and Shearer and Papike (1993) as "green B." Significantly, the Ca/Al values of these two compositions (Table 8, Cols. E and F) are the same. Other similar VLT compositions include some of the volcanic glasses that have been found in other mafic lunar meteorites, especially a picritic glass in QUE94281 (Table 8, Col. G). This composition has slightly higher Al and thus significantly lower Ca/Al, and it has significantly higher Cr than the inferred OC parent-melt composition. Other VLT glass compositions tend to have still higher Al and much lower Mg, e.g., Table 8, Cols. H and I.

The components of NWA773, even though brecciated, appear to be similar to derivative compositions expected from a common VLT picritic precursor, and other related compositions occur in lunar mafic meteorites QUE94281 (and launch-paired Yamato 96008) and EET87521. Korotev et al. (2003) concluded that this group of meteorites may have come from the same region of the Moon or at least formed by a common process, one for which the crystalline volcanic products were not sampled by Apollo and Luna missions, although VLT volcanic glasses occur in regolith at all of the Apollo landing sites (summarized by Shearer and Papike, 1993).

A key feature of NWA773 is its LREE-enriched REE pattern, which is similar to that of KREEP, compared to most mare basalts in the sample collection that also have high FeO and very low TiO_2. Most of the sampled crystalline VLT basalts have flat or LREE-depleted patterns with minor negative Eu or even positive Eu (Luna 24) anomalies (Papike et al., 1998). The LREE enrichment in NWA773 is seen in the bulk, chondrite-normalized REE patterns of both lithologies. Using La/Yb as a measure of LREE/HREE enrichment, the bulk OC and breccia lithologies are 3.8 and 3.1, compared to 3.1 for KREEP (at only one tenth the concentration of KREEP). A key question is whether or not the silicates in OC also record having been in equilibrium with an LREE-enriched melt. Dividing measured REE concentrations by appropriate distribution coefficients yields an estimate of the REE concentrations of contemporary melt at the time the minerals crystallized. We note that this calculation does not yield the *parent* melt composition and that once a pocket of melt is trapped and cut off from communication with the contemporary melt, this calculation is no longer valid. For these calculations we used the ion microprobe REE analyses of pyroxene and plagioclase that, from other lines of evidence, formed earliest, reasoning that these are the most likely to represent contemporary melt at the time of crystallization and not a more evolved composition of trapped melt. Details of these calculations are given in the caption to Figure 16. The results yield REE concentrations that are approximately 200 × chondritic for La, 100 × chondritic for Sm, and 40 × chondritic for Yb. The HREE concentrations of the equilibrium melt calculated from cumulus olivine HREE concentrations, which appear not to have been affected by contamination, indicate similar HREE concentrations to those calcu-

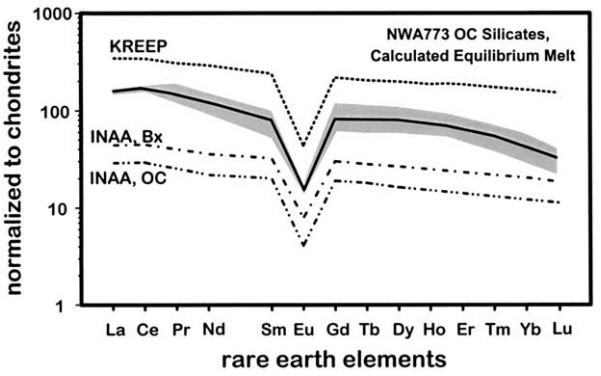

Fig. 16. Calculated REE pattern of melt that was in equilibrium with cumulus pyroxene and plagioclase in NWA773 OC compared to bulk patterns. The pattern defined by these minerals is KREEP-like, but even steeper in terms of LREE/HREE. The pattern was defined using the "least evolved" (lowest REE) patterns determined for each mineral (pigeonite Px 4, augite Px 2, and plagioclase Plas core) by SIMS coupled with distribution coefficients relevant to specific mineral compositions. Distribution coefficients are from McKay et al. (1986) for trivalent REE in pyroxene and McKay et al. (1990) for Eu, and from McKay (1982) for plagioclase. Olivine (not shown) has HREE concentrations that, when coupled with distribution coefficients (McKay, 1986), indicates a melt composition similar to the one shown here. LREE in olivine, however, are strongly enriched relative to what would be in equilibrium with this melt composition; however, the high LREE values appear to result terrestrial contamination as discussed in text.

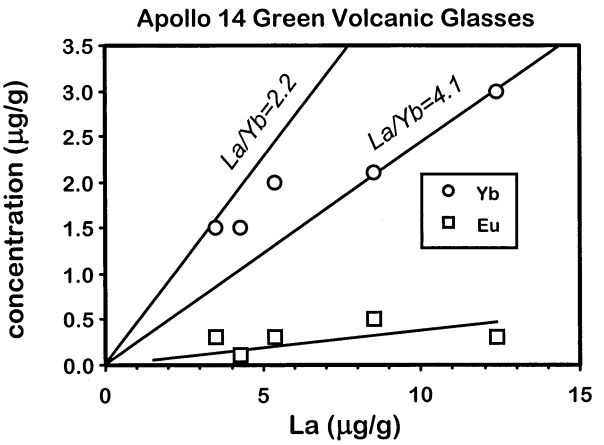

Fig. 17. La vs. Yb and Eu in Apollo 14 volcanic green glasses (data from Shearer and Papike, 1993).

lated from pyroxene, but contamination prevents any conclusions regarding the LREE from olivine analyses.

Two important points can be made with regard to the LREE enrichment. First, the enrichment in OC is indigenous to that lithology as reflected by the REE contents of its unaltered silicates. The calculation of the equilibrium melt described above used the pyroxene and plagioclase REE analyses for the grains that formed earliest (highest temperature pyroxene and plagioclase core). Because all of the silicates record relative LREE/HREE enrichment, it can not result from mixing of some KREEP-rich liquid with an already solid or mostly solid cumulate, nor is it due to the incorporation of a cryptic KREEP component into the breccia. Second, the two NWA773 lithologies, OC and Bx, have very similar REE patterns, differing only in concentration, with Bx slightly higher than OC (e.g., 45 vs. 30 × chondrite at Ce). The similarity of patterns but differing REE concentrations (and major elements, e.g., Mg') between the two lithologies (Tables 1,3) is consistent with a relationship wherein OC represents a less evolved cumulate and Bx represents a more evolved set of volcanic products, which is consistent with their major-element systematics. According to this scenario, the regolith-breccia components consist largely of debris from the erupted parts of the volcanic system.

7.4. Petrogenesis

Pyroxene compositions record information about the crystallization interval, and in the following, we take crystallization to have occurred under low pressure conditions on the basis of lack of coarse exsolution in this composition range. Quadrilateral compositions of pyroxene grains analyzed for trace elements are consistent with the following scenario. The high-T end of the crystallization interval was 1200°C, recorded by pigeonite, Wo_{16}. This grain yielded the lowest REE concentrations of the three pigeonite grains IP 4, IP 5, and IP 7, and REE concentrations increase in the order IP4→IP5→IP7. Although variations in the equilibrium melt REE concentrations calculated for each pyroxene grain (accounting for Wo in the calculation of D values) do not correlate as one might expect for incompatible elements (i.e., increasing concentration with falling temperature and crystallization of olivine, pyroxene, and plagioclase), the equilibrium melt patterns are for the most part similar. This situation is consistent with the pyroxene grains having been mostly cumulus and having formed from a dynamic and probably large reservoir, and over a range of temperatures. Once communication between contemporary melt became limited by crystal growth and then cut off, trapping pockets of residual melt, the melt pockets became progressively enriched in incompatible elements, as reflected by the compositions of the plagioclase rim, pyroxene grain IP 3, and RE-merrillite. Pyroxene compositions record a lower limit to the crystallization interval at about 1050°C according to a plot of compositions on the Sack and Ghiorso (1994) pyroxene quadrilateral with isotherms (Fig. 9).

How and where did the components of NWA773 obtain their incompatible-element enrichment? We have already shown on the basis of major elements that a connection likely exists between the parent melt inferred for the OC lithology and picritic volcanic green glass such as the variety found in Apollo 14 samples, green glass B, listed by Shearer and Papike (1993) in their Table 1 (columns 7a, 7b, 7c, and 8). These volcanic glasses are relatively REE rich compared to other VLT volcanic glasses and they are fractionated in terms of LREE/HREE (La ~ 10 × chondritic, La/Yb = 2.3 to La ~ 35 × chondritic, La/Yb = 4.1 (Fig. 17).) Because these are volcanic glasses and thus did not experience crystal fractionation en route to the surface (and probably no assimilation, either) implies that their REE characteristics were obtained in the mantle source regions (Shearer and Papike, 1993), which are inferred to be some 400–500 km deep or more on the basis of multiple-saturation considerations (Longhi, 1992; Elkins et al., 2000). Still, these REE concentrations are not high enough to produce the OC

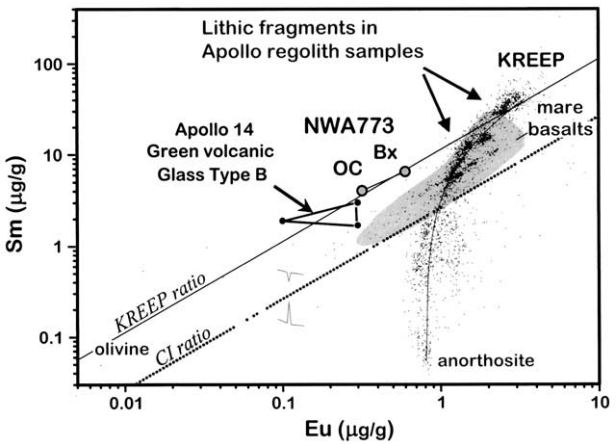

Fig. 18. Geochemical mixing relationships for known lunar materials, NWA773 OC and Bx can only be explained as mixtures of very-low-Ti mantle source materials such as the Apollo 14 picritic glasses and a KREEP component. Shaded field is that of crystalline mare basalts. Above the dotted line marked CI ratio, the Eu anomaly is negative. Apollo 14 Green Glass Type B compositions are shown by the triangle (Sm and Eu concentrations from Shearer and Papike, 1993, their Table 1, column 7 and 8 analyses). The implication of this plot is that the field marked by these Apollo 14 green glass compositions marks a plausible parent melt composition for the components of NWA773.

equilibrium-melt concentrations, even after 50% fractional crystallization. Further assimilation of incompatible-element-rich material is required or the mantle source must have been three times richer in LREE than any of the analyzed VLT volcanic glasses. The simplest explanation is that the NWA773 parent melt assimilated such a component before its rise through the crust and emplacement near the Moon's surface. Given the known range of Apollo 14 VLT volcanic glass REE contents, some 15–30% of material with a KREEP-like composition would have to have been assimilated. Figure 18 shows the mixing relationship between NWA773 OC (and Bx) components, Apollo 14 volcanic green glass, and KREEP. The plot of Sm vs. Eu shows that the NWA773 composition differs from typical lunar basalt compositions in a way that is consistent with mixing of the Apollo 14 VLT volcanic glass composition with an incompatible-element-rich component with KREEP-like trace-element signature. This mixing relationship is also consistent with the olivine enrichment and low-Ti character of NWA773.

To generate a residual melt with LREE/HREE as high as (or possibly slightly greater than) KREEP, such as appears to have been the case for the OC equilibrium melt (residual, not parental), either the mantle source region or the assimilated incompatible-element-rich component must have had a high LREE/HREE to begin with. Either case requires extended magmatic differentiation relative to that commonly ascribed to early magma-ocean solidification when deep mantle sources were likely formed. Several known lunar crustal materials have high REE concentrations and LREE/HREE as high as or greater than KREEP. Primarily these are the compositionally evolved monzogabbros (also referred to as monzodiorite or quartz monzodiorite) found at several Apollo landing sites (Snyder et al., 1995; Jolliff, 1998). Compositions of other REE-enriched basalts found at Apollo 14 have been attributed to assimilation of a KREEP component (e.g., Shervais et al., 1984, 1985; Dickinson et al., 1985)

The low Ti content inferred for the source region and parent melt of NWA773 components provides a potential constraint on the origin of the geochemical signature. The low Ti concentration relative to the expected residua of extensive lunar magma-ocean differentiation suggests a source that was enriched in REE (and had high LREE/HREE), yet was depleted of late-stage ilmenite perhaps through prior loss of a dense ilmenite-bearing crystal fraction to gravitational separation (Hess and Parmentier, 1995). Segregations of residua rich in the phosphate RE-merrillite, which has both high REE concentrations and LREE/HREE typically equal to or slightly greater than KREEP (Jolliff et al., 1993), may have existed at different levels within the crust, or dense, late-stage magma-ocean residua may have sunk into the upper mantle as they continued to fractionate, leaving local regions enriched in either ilmenite or phosphate. A mixing scenario involving overturn/hybrid mantle remelting (but not crustal assimilation) is consistent with interpretations of Elkins et al. (2000) on the basis of phase equilibria. The NWA773 parent melt either mixed with (in the source region) or assimilated (on the way up) material enriched in the phosphate fraction. Such material would have been hot because of its high concentration of Th, which is also strongly concentrated in RE-merrillite, so the assimilation process may not have been a severe impediment to further rise of the parent melt.

Regarding incompatible trace elements other than the REE, in NWA773 some of the large-ion lithophile elements (e.g., Rb, Cs, Th, U) are not as enriched as the LREE compared to KREEP. This lack of uniform enrichment of incompatible trace elements may relate to enrichment in an RE-merrillite-rich residue at some point in the petrogenesis of NWA773 components. On the other hand, K and Ba appear to be slightly enriched, consistent with or slightly exceeding LREE concentrations relative to KREEP. The potential enrichment of K and Ba in particular, as a result of terrestrial contamination, make further speculation about differential LIL enrichments or depletions unwarranted.

Although the details of the broader process of LREE/HREE enrichment of the source region for NWA773 components remain speculative, it seems clear that differentiation needed to produce the enrichment must have involved mixing and remelting of materials of the upper mantle or lower crust. On Earth, repetition of such cycles, owing to plate tectonics, has produced a crust with distinctive LREE/HREE enrichment. On the Moon, this kind of differentiation probably occurred on a large scale only in the Procellarum KREEP Terrane (Haskin et al., 2000), where sufficient Th, U, and K were concentrated so as to promote igneous activity of extended duration.

Thorium, in particular, has special significance because its surface distribution has been mapped globally by the Lunar Prospector γ-ray spectrometer (Lawrence et al., 2000), including basalt-rich areas such as many that occur within the Procellarum KREEP Terrane (Jolliff et al., 2001). At the time of trapping of residual melt within the crystallizing NWA773 OC precursor (at equilibrium with pyroxene and plagioclase), by analogy with the REE, Th would have been ~ 5 μg/g if it behaved like the HREE, but could have been higher (up to 9

μg/g if it behaved more like LREE). If such a melt composition were to erupt to the surface, it would be a good candidate for a Th-enriched basalt such as may occur in parts of the Procellarum region on the basis of remotely sensed Th data (Lunar Prospector γ-ray spectrometer). This possibility has added significance if the age of OC and the breccia are as young as indicated by ^{40}Ar-^{39}Ar dating ($\sim$2.7 Ga; Fernandes et al., 2002, 2003). Many of the basalts of Western Procellarum that appear from the remotely sensed data to be Th-rich also have intermediate to high Ti contents; however, potential VLT source regions appear to be scarce in the Procellarum region and near the Apollo 14 site (Gillis et al., 2003).

In summary, the following points may be made with respect to the petrogenesis of NWA773 components. From an Apollo 14 green volcanic-glass bulk composition (very low TiO_2 and MgO-rich), low-pressure crystallization produces about 40% by mass olivine (on average, the model olivine has the same Fo content as measured OC olivine) and an equilibrium melt, when it reaches pyroxene and plagioclase saturation, that (1) produces calcic pyroxene (pigeonite and augite) and (2) has a composition very much like what is needed to produce the OC silicate assemblage and compositions. In terms of trace elements, however, the parent melt of NWA773 OC must be enriched in incompatible elements, especially REE, before olivine crystallization/accumulation. In support of this timing, IMP analyses of HREE in olivine in OC coupled with mineral/melt distribution coefficients yield equilibrium-melt HREE concentrations that are consistent with those calculated from the lowest of the plagioclase and pyroxene REE concentrations, e.g., 40–80 $\times$ chondrite values. Furthermore, the removal of 30–40% olivine essentially increases REE concentrations in the residual melt by $\sim$40–50%. To reach the REE concentrations of melt calculated to have been in equilibrium with the silicates in the NWA773 olivine cumulate requires assimilation of some 20% by mass of KREEP of the high-K (Warren, 1988) or average mafic IMB (Jolliff, 1998) composition to as little as 10% if the composition of the assimilant is that of RE-merrillite-rich ferrogabbro (e.g., Jolliff, 1998). The latter composition, as a late-stage differentiate of the magma ocean (urKREEP) following separation of dense Ti-rich cumulates, is perhaps more likely (than average high-K KREEP) to have been encountered by a rising VLT magma deep in the crust or in the upper mantle.

7.5. Similarity of Composition to EET87521/96008

Although Ti-rich basalt is common in the Apollo collection, basalts of low-Ti composition are far more common on the Moon, as reflected by Clementine global remote sensing (Giguere et al., 2000; Gillis et al., 2003) and as sampled by the basaltic lunar meteorites thus far. NWA773 bears major-element and petrographic similarities to other lunar basaltic meteorites, especially in the diversity of VLT basaltic components and in terms of pyroxene textures. Several meteorites such as Yamato 793274 and QUE94281 "YQ" and EET87/96 (87521, 96008) ("EET") (Arai et al., 1996; Arai and Warren, 1999; Korotev et al., 2003) contain fragments of compositionally zoned and relatively coarse-grained pyroxene, in many cases exhibiting fine exsolution lamellae. Although the latter do not reflect the slow cooling expected from crystallization at depth (e.g., McCallum and O'Brien, 1996), the observation that most mare basalt samples do not show such exsolution indicates that the VLT gabbros (including the olivine cumulate of NWA773) represent hypabyssal igneous bodies. The similarity in composition between the hypabyssal rocks and erupted counterparts indicates that they are generally part and parcel of the same magma systems. In terms of trace elements, it is noteworthy that the YQ and EET lunar meteorites also have high incompatible-element concentrations and LREE/HREE relative to most mare basalts, with La/Yb in the 2.5–2.75 range. In the case of YQ, substantial admixed nonmare components also contribute to the bulk incompatible-element signature and thus obscure trace-element enrichments of the volcanic components. Trace-element studies of the volcanic components of these meteorites by methods such as ion microprobe or laser-ablation ICP-MS are needed to further investigate the possible connections between these and NWA773.

7.6. Connection to Magnesian Suite Igneous Rocks?

Previous studies of rocks such as troctolite 76535 (e.g., Haskin et al., 1974) showed that the trace-element contents (trapped melt components) of some magnesian-suite rocks indicated crystallization from evolved equilibrium melts (and their inferred parent melts) relative to the ferroan anorthosites. The application of the ion microprobe to determine trace-element contents of the major silicate minerals, coupled with equilibrium mineral/melt distribution coefficients, confirmed the idea that many of the magnesian-suite cumulates, even those lacking a trapped-melt component, must have formed from trace-element-rich equilibrium melts (Papike et al., 1994, 1996; Shervais and McGee, 1998), e.g., 0.7 to 2 times high-K KREEP. Here, we explore the possibility that the NWA773 olivine cumulate is related to the magnesian-suite rocks, as suggested by Bridges et al. (2002).

Incorporation of a KREEP component into a low-Ti melt, generated by partial melting in the mantle, is similar to an explanation that has been put forth recently for the origin of magnesian-suite intrusive rocks (e.g., Korotev, 2000; Hess, 2000). Mineral compositions in terms of plagioclase An content and Mg' of mafic silicates in NWA773 OC span the magnesian-suite field and project toward the field typical of mare basalts. Similarities in mineral compositions led Bridges et al. (2002) to suggest an affinity between NWA773 and the magnesian intrusive rock suite. A connection between VLT mare basalts and magnesian-suite intrusives seems unlikely owing to big differences in Ca/Al (see Longhi, 1981), with magnesian-suite magmas following the crystallization sequence olivine $\rightarrow$ plagioclase $\rightarrow$ low-Ca pyroxene $\rightarrow$ high-Ca pyroxene. Also, Ni and Co concentrations in olivine and in the bulk OC are much higher than in the olivine of magnesian-suite rocks (Shearer and Papike, 2000), suggesting further, fundamental petrogenetic differences.

Still, NWA773 presents an interesting case for comparison because of the apparent incorporation of KREEP-like material in its petrogenesis and in the petrogenesis of magnesian-suite rocks. That this igneous process, i.e., the incorporation of Th-U-K-rich material into different mantle source regions over a range of depths and source composition could have extended from the age of the most ancient magnesian-suite rocks to the

time of mare-basalt generation and perhaps even to as young as ~3 Ga is remarkable, if correct. Such a prolonged interval of magmatic activity further suggests localization to the western nearside Procellarum KREEP Terrane where elevated concentrations of heat-producing Th, U, and K may have pervaded the crustal section and parts of the underlying upper mantle (Jolliff et al., 2000) and so enhanced melting, mixing, and continued injection of melts into the crust over time. The similarity between the parent melt we infer for NWA773 OC and picritic glasses found at the Apollo 14 site strengthens the possibility that NWA773 comes from a site within the Procellarum KREEP Terrane.

8. CONCLUSIONS

Lunar meteorite NWA773 is essentially a dimict breccia consisting of two main lithologies, an olivine-gabbro cumulate and a mafic, gabbroic volcanic breccia probably of mare origin, judging by the paucity of nonmare lithologic components. Both lithologies have Fe-rich and Al-poor compositions that relate them to known VLT mare-basalt compositions, and they share trace-element characteristics specifically of LREE/HREE enrichment that are unusual for lunar volcanic rocks of such low Ti content. Unlike Apollo mare basalts, both lithologies of NWA773 have generally KREEP-like relative concentrations of incompatible elements, yet modest absolute concentrations. The OC lithology contains cumulus olivine and appears also to have excess pyroxene relative to plagioclase, compared to cotectic proportions of these minerals. Mineral compositions and pyroxene exsolution features require a shallow, hypabyssal origin for OC and for some of the clasts in the breccia matrix. Other clasts in the breccia matrix are consistent with volcanic and regolith components at the lunar surface. Although some of the fine-grained materials in the glassy matrix resemble agglutinates, the coarseness of mineral and lithic clasts that were incorporated into the breccia matrix, the paucity of volcanic glass beads, and the low meteoritic siderophile-element abundances indicate an immature surface in the source region or that the specific ejecta that became NWA773 simply did not incorporate much surface regolith.

Terrestrial alteration is present in NWA773 and must be taken into account in assessment of bulk and mineral compositions. Fracture-filling calcite in NWA773 is abundant and contributes to the apparently high bulk Ca/Al of the meteorite. Even so, the high proportion of Ca-rich pyroxene, including both augite and pigeonite, reflects an intrinsically high Ca/Al that is typical of lunar mare basalts compared to known nonmare crustal rock types. Concentrations of elements commonly associated with carbonate deposits such as Sr and Ba are elevated in some mineral analyses, such as in olivine, where intrinsic concentrations of these elements ought to be extremely low. These elements, however, are not significantly enriched in the bulk meteorite, providing an overall constraint on the level of compositional contamination. Terrestrial contamination also accounts for LREE enrichment seen in some of the ion microprobe analyses of olivine and low-Ca pyroxene, but the contamination may be traced to fine-grained terrestrial deposits in fracture fillings. The magnitude of contamination is insufficient to affect other minerals, including plagioclase, clinopyroxene, and RE-merrillite. On the basis of analyses of these minerals, NWA773 OC formed from a magmatic precursor that was enriched in LREE/HREE compared to most lunar mare basalts.

On the basis of compositional similarities and petrogenetic modeling, the volcanic breccia components of NWA773 appear to be related to the olivine cumulate lithology, as concluded also by Fagan et al. (2003). The parent melt that produced the OC cumulate was similar to known Apollo 14 VLT picritic glasses. Melt of this composition, generated at a depth of some 400 km, could produce the observed compositions by mixing with a KREEP-like component in the upper mantle or crust enroute to the surface or where magma intruded or ponded near the surface. Solidification and differentiation of this melt in a shallow body produced other, more chemically evolved components that became separated either laterally or vertically from OC, but which were subsequently incorporated into overlying regolith and included in the breccia matrix.

If the petrogenetic scenario described above, with a connection to Apollo 14 VLT glasses is correct, then NWA773 represents an unusual case for lunar mare basalts and a fruitful target for further study. NWA773 appears to provide a link between a specific picritic glass group (Apollo 14, group B), generated deep in the lunar mantle, a shallow intrusive differentiate of such melt that did not erupt, and related volcanic components from the surface. Although volcanic glass beads in NWA773 appear to be scarce, the finding and analysis of such beads, especially with a VLT picritic composition and trace-element enrichment, would strengthen the apparent relationship and would help to determine at what depth the incompatible-element contamination occurred. Further study of the trace-element characteristics of volcanic components in the breccia matrix is needed to verify petrogenetic connections inferred from bulk compositions between OC and breccia-matrix components.

In a broader comparison, the inferred relationships between volcanic glass, gabbroic, and basaltic components in NWA773 are similar to what have been found in other lunar mare meteorites such as QUE94281 (and probably EET87/96), where candidates for related volcanic glasses and crystalline components appear to occur in the same breccia. On an even broader scale, NWA773, with its unusual LREE/HREE enrichment, KREEP-like signature, and apparent relationship to Apollo 14 green picritic glasses, supports a source in the Procellarum KREEP Terrane, and possibly one near the Apollo 14 site, even though obvious VLT volcanic sources appear to be scarce in this region. Comparison of the intrusive OC lithology to magnesian-suite intrusives may provide further insights and connection to a common origin from mantle-derived VLT magmas that also incorporated KREEP deep in the lower crust or upper mantle.

Acknowledgments—Support for this work came primarily from NASA grant NAG5-4172 (L. Haskin). We thank Monica Grady and the Natural History Museum of London for providing samples of NWA773. We thank Tim Fagan for providing a preprint of his manuscript and for discussion of the features of NWA773. We are grateful to Marvin Killgore for making portions of this meteorite available to the scientific community for study. Detailed and very useful critical reviews of the manuscript provided by Paul Warren and Tim Fagan, and additional comments and editorial handling by associate editor Duck Mittlefehldt, led to significant improvements and are much appreciated. Finally, we acknowledge and thank Bob Walker for inspiration and for his pioneering contributions to Apollo-Program science

and his dedication to use of the ion microprobe to study extraterrestrial materials.

Associate editor: D. W. Mittlefehldt

REFERENCES

Anders E. and Grevesse N. (1989) Abundances of the elements: Meteoritic and solar. *Geochim. Cosmochim. Acta* **53,** 197–214.

Arai T. and Warren P. H. (1999) Lunar meteorite Queen Alexandra Range 94281: Glass compositions and other evidence for launch pairing with Yamato 793274. *Meteorit. Planet. Sci.* **34,** 209–234.

Arai T., Takeda H., and Warren P. H. (1996) Four lunar mare meteorites: Crystallization trends of pyroxenes and spinels. *Meteorit. Planet. Sci.* **31,** 877–892.

Armstrong J. T. (1988) Quantitative analysis of silicate and oxide minerals: Comparison of Monte-Carlo, ZAF, and phi-rho-Z procedures. *Microbeam Analysis* **23,** 239–246.

Bence A. E. and Papike J. J. (1972) Pyroxenes as recorders of lunar basalt petrogenesis: Chemical trends due to crystal-liquid interaction. Proc. 3rd Lunar Sci. Conf. (Suppl. 3), *Geochim. Cosmochim. Acta* **1,** 431–469.

Bridges J. C., Jeffries T. E. and Grady M. M. (2002). Trace element signatures of trapped KREEP in olivine- rich clasts within lunar meteorite NWA773, abstract #5137. *Meteorit. Planet. Sci*. **37,** No. 7, (Suppl.), A24.

Crozaz G. and Wadhwa M. (2001) The terrestrial alteration of Saharan Shergottites Dar al Gani 476 and 489: A case study of weathering in a hot desert environment. *Geochim. Cosmochim. Acta* **65,** 971–978.

Delano J. W. (1986) Pristine lunar glasses: Criteria, data, and implications. Proc. 16th Lunar Planet. Sci. Conf., Part 2. *J. Geophys. Res.* **91,** D201–D213.

Dickinson T., Taylor G. J., Keil K., Schmitt R. A., Hughes S. S. and Smith M. R. (1985) Apollo 14 aluminous mare basalts and their possible relationship to KREEP. Proc. 15th Lunar Planet. Sci. Conf. *J. Geophys. Res.* **90,** (Suppl.) C365–C374.

Dymek R. F., Albee A. L. and Chodos A. A. (1975) Comparative petrology of lunar cumulate rocks of possible primary origin: Dunite 72415, troctolite 76535, norite 78235 and anorthosite 62237. Proc. 6th Lunar Sci. Conf., pp. 301–341.

Elkins L. T., Fernandes V. A., Delano J. W., and Grove T. L. (2000) Origin of lunar ultramafic green glasses: Constraints from phase equilibrium studies. *Geochim. Cosmochim. Acta* **64,** 2339–2350.

Eugster, O. and Lorenzetti S. (2001). Exposure history of some differentiated and lunar meteorites. *Meteorit. Planet. Sci.* **36,** No. 9 (Suppl.), A54-A55.

Fagan T. J., Keil K., Taylor G. J., Hicks T. L., Killgore M., Bunch T. E., Wittke J. H., Eugster O., Lorenzetti S., Mittlefehldt D. W., Clayton R. N., and Mayeda T. (2001) New lunar meteorite Northwest Africa 773: Dual origin by cumulate crystallization and impact brecciation (abstract #5149). *Meteorit. Planet. Sci.* **36, (***Suppl.***)**, A55.

Fagan T. J., Taylor G. J., Keil K., Hicks T. L., Killgore M., Bunch T. E., Wittke J. H., Mittlefehldt D. W., Clayton R. N., Mayeda T., Eugster O., Lorenzetti S., and Norman M. D. (2003) Northwest Africa 773: Lunar origin and iron-enrichment trend. *Meteorit. Planet. Sci.* **38,** 529–554.

Fernandes V. A., Burgess R. and Turner G. (2002) Northwest Africa 773 (NWA773): ^{40}Ar-^{39}Ar studies of breccia and cumulate lithologies. *Workshop on The Moon Beyond. 2002, Next Steps in Lunar Science and Exploration.* Abstract #3033, September 12–14, 2002, Taos, New Mexico.

Fernandes V. A., Burgess R., and Turner G. (2003) ^{40}Ar-^{39}Ar chronology of lunar meteorites Northwest Africa 032 and 773. *Meteorit. Planet. Sci.* **38,** 555–564.

Floss C. (2000) Complexities on the acapulcoite-lodranite parent body: Evidence from trace element distributions in silicate minerals. *Meteorit. Planet. Sci.* **35,** 1073–1085.

Floss C. and Crozaz G. (1991) Ce anomalies in the LEW85300 eucrite: Evidence for REE mobilization during Antarctic weathering. *Earth Planet. Sci. Lett.* **107,** 13–24.

Floss C, Crozaz G (2001) Terrestrial alteration of lunar meteorites Dar al Gani 262 and 400. *Lunar Planet. Sci. XXXII* Lunar Planet. Inst., Houston. #1105 (abstr.).

Foley R. T., Druck J. U., and Fryxell R. E. (1955) The oxidation of iron-nickel alloys. *J. Electrochem. Soc.* **102 (***8***),** 440–445.

Giguere T. A., Taylor G. J., Hawke B. R., and Lucey P. G. (2000) The titanium contents of lunar mare basalts. *Meteor. Planet. Sci.* **35 (1),** 193–200.

Gillis J. J., Jolliff B. L. and Elphic R. C. (2003) A revised algorithm for calculatingTiO2 from Clementine UVVIS data: A synthesis of rock, soil and remotely sensed TiO_2 concentrations. *J. Geophys. Res.*, 108(E2), 10.1029/2001JE0 01515.

Grossman J. N., Zipfel J. (2001) The Meteoritical Bulletin, No. 85, September., *Meteorit. Planet. Sci.* **36,** *(9),* (Suppl.) A300.

Haskin L. A., Shih C.-Y., Bansal B. M., Rhodes J. M., Weismann H. and Nyquist L. E. (1974) Chemical evidence for the origin of 76535 as a cumulate. Proc. 5th Lunar Sci. Conf., pp. 1213–1225.

Haskin L. A., Gillis J. J., Korotev R. L., and Jolliff B. L. (2000) The materials of the lunar Procellarum KREEP Terrane: A synthesis of data from geomorphological mapping, remote sensing, and sample analyses. *J. Geophys. Res.* **105,** 20403–20415.

Hess P. C. (2000) On the source regions for mare picritic glasses. *J. Geophys. Res.* **105,** *(E2),* 4347–4360.

Hess P. C. and Parmentier E. M. (1995) A model for the thermal and chemical evolution of the Moon's interior: Implications for the onset of mare volcanism. *Earth Planet. Sci. Lett.* **134,** 501–514.

Hess P. C., Horzempa P., Rutherford M. J., and Devine J. (1990) Phosphate equilibria in lunar basalts. *Lunar and Planetary Science* **XXI,** 505–506.

Jolliff B. L. (1998) Large-scale separation of K-frac and REEP-frac in the source regions of Apollo impact-melt breccias and a revised estimate of the KREEP composition. *International Geology Review* **10,** 916–935.

Jolliff B. L., Korotev R. L., and Haskin L. A. (1991) Geochemistry of 2–4 mm particles from Apollo 14 soil (14161) and implications regarding igneous components and soil-forming processes. *Proceedings of Lunar and Planetary Science* **21,** 193–219.

Jolliff B. L., Haskin L. A., Colson R. O., and Wadhwa M. (1993) Partitioning in REE-saturating minerals: Theory, experiment, and modelling of whitlockite, apatite, and evolution of lunar residual magmas. *Geochim. Cosmochim. Acta* **57,** 4069–4094.

Jolliff B. L., Rockow K. M., and Korotev R. L. (1998) Geochemistry and petrology of lunar meteorite Queen Alexandra Range 94281, a mixed mare and highland regolith breccia, with special emphasis on very-low-Ti mafic components. *Meteorit. Planet. Sci.* **33,** 581–601.

Jolliff B. J., Floss C., McCallum I. S., and Schwartz J. M. (1999) Geochemistry, petrology, and cooling history of 14161,7373: A plutonic lunar sample with textural evidence of granitic-fraction separation by silicate-liquid immiscibility. *Am. Mineral.* **84,** 821–837.

Jolliff B. L., Gillis J. J., Haskin L., Korotev R. L., and Wieczorek M. A. (2000) Major lunar crustal terranes: Surface expressions and crust-mantle origins. *J. Geophys. Res.* **105,** 4197–4216.

Jolliff B. L., Gillis J. J., Lawrence D. J. and Maurice S. (2001) Thorium content of mare basalts of the western Procellarum region. *Lunar and Planetary Science* **XXXII,** #2144.

Karner J., Papike J. J., and Shearer C. K. (2003) Olivine from planetary basalts: Chemical signatures that indicate planetary parentage and those that record igneous setting and process. *Am. Mineral.* **88,** 806–816.

Korotev R. L. (1991) Geochemical stratigraphy of two regolith cores from the central highlands of the Moon. *Proc. Lunar Planet. Sci. Conf.* **21,** 229–289.

Korotev R. L. (1996) A self-consistent compilation of elemental concentration data for 93 geochemical reference standards. *Geostandards Newsletter* **20,** 217–245.

Korotev R. L. (2000) The great lunar hot spot and the composition and origin of the Apollo mafic ("LKFM") impact-melt breccias. *J. Geophys. Res.* **105,** 4317–4345.

Korotev R. L., Zeigler R. A., Jolliff B. L. and Haskin L. A. (2002) Northwest Africa 773–. An unusual rock from the lunar maria, abstract #5259. *Meteorit. Planet. Sci*. **37,** No. 7 (Suppl.), A81.

Korotev R. L., Jolliff B. L., Zeigler R. A. and Haskin L. A. (2003). Compositional constraints on the launch pairing of three brecciated lunar meteorites of basaltic composition. *Antarctic Meteorite Research* **16,** 152–175.

Laul J. C. and Schmitt R. A. (1973) Chemical composition of Apollo 15, 16 and 17 samples. Proc. 4th Lunar Sci. Conf., pp. 1349–1367.

Lawrence D. J., Feldman W. C., Barraclough B. L., Binder A. B., Elphic R. C., Maurice S., Miller M. C., and Prettyman T. H. (2000) Thorium abundances on the lunar surface. *J. Geophys. Res.* **105,** 20307–20331.

Longhi J. (1981) Preliminary modeling of high pressure partial melting: Implications for early lunar differentiation. *Proceedings of the Twelfth Lunar and Planetary Science Conference, Part B.* pp. 1001–1018.

Longhi J. (1987) On the connection between mare basalts and picritic glasses. Proc. 17th Lunar Planet. Sci. Conf., Part 2. *J. Geophys. Res.* **92,** E349–E360.

Longhi J. (1991) Comparative liquidus equilibria of hypersthene-normative basalts at low pressure. *American Mineralogist* **76,** 785–800.

Longhi J. (1992) Experimental petrology and petrogenesis of mare volcanics. *Geochim. Cosmochim. Acta* **56,** 2235–2251.

Longhi J. and Pan V. (1988) A reconnaissance study of phase boundaries in low-alkali basaltic liquids. *Journal of Petrology* **29,** 115–147.

McCallum I. S. and O'Brien H. E. (1996) Stratigraphy of the lunar highland crust: Depth of burial of lunar samples from cooling rate studies. *American Mineralogist* **81,** 1166–1175.

McKay G. A. (1982) Partitioning of REE between olivine, plagioclase, and synthetic melts: Implications for the origin of lunar anorthosite. *Lunar and Planetary Science* **XIII,** 493–494.

McKay G. A. (1986) Crystal/liquid partitioning of REE in basaltic systems: Extreme fractionation of REE in olivine. *Geochim. Cosmochim. Acta* **50,** 69–79.

McKay G. A. and Weill D. F. (1976) Petrogenesis of KREEP. *Proceedings of the 7th Lunar Science Conference.* pp. 2427–2447.

McKay G., Wagstaff J., and Yang S.-R. (1986) Clinopyroxene REE distribution coefficients for shergottites: The REE content of the Shergotty melt. *Geochim. Cosmochim. Acta* **50,** 927–937.

McKay G. A., Wagstaff J. and Le L. (1990) REE distribution coefficients for pigeonite: Constraints on the origin of the mare basalt europium anomaly. *Workshop on Lunar Volcanic Glasses: Scientific and Resource Potential* (ed. J. W. Delano and G. H. Heiken), LPI Tech. Rpt. 90–02, pp. 48–49.

Morse S. A. (1984) Cation diffusion in plagioclase feldspar. *Science* **225,** 504–505.

Papike J. J. (1998) Comparative planetary mineralogy: Chemistry of melt-derived pyroxene, feldspar and olivine. In *Planetary Materials*, Vol. 36 (ed. J. J. Papike), Mineralogical Society of America, pp. 7–1–7–11.

Papike J. J., Fowler G. W., and Shearer C. K. (1994) Orthopyroxene as a recorder of lunar crust evolution: Am ion microprobe investigation of Mg-suite norites. *American Mineralogist* **79,** 796–800.

Papike J. J., Fowler G. W., Shearer C. K., and Layne G. D. (1996) Ion microprobe investigation of plagioclase from lunar Mg-suite norites: Implications for calculating parental melt REE concentrations and for assessing post-crystallization REE distribution. *Geochim. Cosmochim. Acta* **60,** 3967–3978.

Papike J. J., Ryder G. and Shearer C. K. (1998) Lunar Samples. In *Reviews in Mineralogy*, Vol. 36, *Planetary Materials* (ed. J. J. Papike), Mineralogical Society of America, Washington, pp. 5–1–5–234.

Rubin A. E. (1997) Mineralogy of meteorite groups. *Meteor. Planet. Sci.* **32,** 231–247.

Ryder G. (1992) Chemical variation and zoning of olivine in lunar dunite: Near-surface accumulation. *Proc. Lunar Planet. Sci.* **22,** 373–380.

Sack R. O. and Ghiorso M. S. (1994) Thermodynamics of multicomponent pyroxenes: II. Phase relations in the quadrilateral. *Contrib. Mineral. Petrol.* **116,** 287–300.

Shearer C. K. and Papike J. J. (1993) Exploring volcanism on the Moon: A perspective from volcanic picritic glass beads. *Geochim. Cosmochim. Acta* **57,** 4785–4812.

Shearer C. K. and Papike J. J. (2000) Compositional dichotomy of the Mg suite. Origin and implications for the thermal and compositional structure of the lunar mantle. *Lunar Planet. Sci. XXXI*, Lunar Planet. Inst., Houston. #1405 (abstr.).

Shervais J. W. and McGee J. J. (1998) Ion and electron microprobe study of troctolites, norite, and anorthosites from Apollo 14: Evidence for urKREEP assimilation during petrogenesis of Apollo 14 Mg-suite rocks. *Geochim. Cosmochim. Acta* **62,** 3009–3023.

Shervais J. W., Taylor L. A., Laul J. C., and Smith M. R. (1984) Pristine highlands clasts in consortium breccia 14305: Petrology and geochemistry. Proc. 15th Lunar Planet. Sci. Conf. *J. Geophys. Res.* **89, (***Suppl.***)** C25–C40.

Shervais J. W., Taylor L. A., and Lindstrom M. M. (1985) Apollo 14 mare basalts: Petrology and geochemistry of clasts from consortium breccia 14321. Proc. 15th Lunar Planet. Sci. Conf. *J. Geophys. Res.* **89, (***Suppl.***)** C375–C395.

Snyder G. A., Taylor L. A., and Halliday A. (1995) Chronology and petrogenesis of the lunar highlands alkali suite: Cumulates from KREEP basalt crystallization. *Geochim. Cosmochim. Acta* **59,** 1185–1203.

Snyder G. A., Taylor L. A. and Patchen A. (1999) Lunar meteorite EET 96008, Part I. Petrology & mineral chemistry: Evidence of large-scale, late-stage fractionation. *Lunar Planet. Sci. XXX*. Lunar Planet. Inst., Houston, #1499(abstr.).

Stöffler D., Knoll H.-D., Marvin U. B., Simonds C. H., and Warren P. H. (1980) Recommended classification and nomenclature of lunar highland rock—A committee report. In *Proceedings of the Conference on the Lunar Highlands Crust* (eds. J. J. Papike and R. B. Merrill), Pergamon Press, New York, pp. 51–70.

Warren P. H (1988) KREEP: Major-element diversity, trace-element uniformity (almost). In *Workshop on Moon in Transition: Apollo 14, KREEP and Evolved Lunar Rocks* (ed. G. J. Taylor and P. H. Warren). LPI Tech. Report. 89–03. Lunar Planet. Inst., Houston. pp. 106–110.

Tanimizu M. and Tanaka T. (2002) Coupled Ce-Nd isotopic systematics and rare earth element differentiation of the Moon. *Geochim. Cosmochim. Acta* **66,** 4007–4014.

Zinner E. and Crozaz G. (1986) A method for the quantitative measurement of rare earth elements in the ion microprobe. *Internat. J. Mass Spectrometry and Ion Processes* **69,** 17–38.